SILICON SOLAR CELL BY LASER PROCESSING TECHNOLOGY

By

MD. NAHID HASAN (132474)
MD. ABDULLAH AL ASIF (132404)
HASAN MD. TANBIN RAHMAN (132468)
MD. NEAZUL HASAN (132440)

A Thesis Submitted to the Academic Faculty in Partial Fulfillment of the Requirements for the Degree of

BACHELOR OF SCIENCE IN ELECTRICAL AND ELECTRONIC ENGINEERING

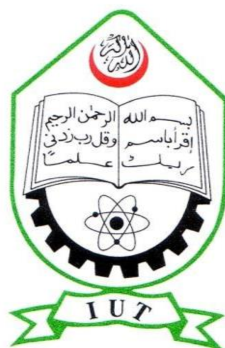

Department of Electrical and Electronic Engineering
Islamic University of Technology (IUT)
Gazipur, Bangladesh

November 2017

SILICON SOLAR CELL BY LASER PROCESSING TECHNOLOGY

Approved by:

Prof Dr. Md. Ashraful Hoque

Professor and Head of the Department,

Department of Electrical and Electronic Engineering,

Islamic University of Technology (IUT),
Boardbazar, Gazipur-1704.

Date: ………………….

Supervised by:

Prof Dr. Md. Ashraful Hoque

Professor and Head of the Department,

Department of Electrical and Electronic Engineering,

Islamic University of Technology (IUT),
Boardbazar, Gazipur-1704.

Date: ………………….

TABLE OF CONTENT

LIST OF FIGURES . . . 4

ACKNOWLEDGEMENT . . . 6

ABSTRACT . . . 7

1 INTRODUCTION . . . 9

1.1 SILICON SOLAR CELLS . . . 11
1.2 MOTIVATION AND OBJECTIVE OF THE THESIS . . . 14
1.3 STRUCTURE OF THE THESIS . . . 16

2 INVESTIGATED TOOLS AND TECHIQUES . . . 17

2.1 LASERS . . . 17
2.2 EXTRACTION OF LASER PARAMETERS . . . 19
2.3 THIN FILM DEPOSITION . . . 22
2.4 MICROSCOPY . . . 22
2.5 WET CHEMICAL PROCESSING . . . 23
2.6 REFERENCE AND TRANSMITTANCE MEASUREMENTS . . . 25
2.7 MINORITY CAREER LIFETIME . . . 26
2.8 SILICON SUBSTRATE . . . 27

3 LASER PROCESSING FOR SILICON SOLAR CELLS . . . 29

3.1 STATE OF LASER PROCESSING FOR SILICON SOLAR CELS . . . 29
3.2 LASER MATERIAL INTERACTION . . . 33
3.3 SIMULATIONS ON LASER-MATERIAL INTERACTION . . . 36
3.3.1 LONG PULSES . . . 37
3.3.2 ULTRASHOT PULSES . . . 39
3.3.3 FREE ELECTRON THEORY . . . 43
3.4 LASER INDUCED DAMAGE . . . 45

4 LIGHT-TRAPPING STRUCTURES IN SILICON SOLAR CELLS . . . 48

4.1 LIGHT MANAGEMENT IN SILICON SOLAR CELLS . . . 48
4.2 STATE OF LASER TEXTURING . . . 52
4.3 MASKED LASER TEXTURING . . . 54

5 DISCUSSION AND OUTLOOK . . . 58

6 CONCLUSION . . . 60

LIST OF FIGURES

Figure1.1: Total installed PV production capacity……………………………………..10

Figure1.2: Illustration of some absorption and loss mechanisms in a solar cell………….12

Figure1.3: Solar irradiance and the maximum available energy. 13

Figure2.1: Surface modifications caused by ultrashort laser pulses………………………19

Figure2.2: Typical set of images used as data…………………………………………21

Figure2.3: (Top) Inverted pyramid structure showing incomplete (left) and complete (right) etching. (Bottom) KOH polishing etch on slurry-sawn wafer (left) and on polished wafer (right)……………………………………………………………………………………25

Figure3.1: Schematic cross-section of a solar cell, highlighting potential areas for laser processing……………………………………………………………………………………32

Figure3.2: Typical process results when irradiating a silicon nitride on silicon stack with long and ultra short laser pulse………………………………………………………………………………..34

Figure3.3: SEM images of complete pieces of SiN_x...35

Figure3.4: intensity distribution through a silicon slab at various times during a laser pulse………………………………………………………………………………………..43

Figure3.5: Theoretical reflectance as function of free electron density in silicon and silicon nitride……………………………………………………………………….……44

Figure3.6: TEM images of silicon wafer irradiated by nanosecond pulses with a wavelength of 1064 nm…………………………………………………………………………….47

Figure4.1: Sketch of a wafer showing various contributions to optical absorption and loss in a solar cell……………………………………………………………………….…49

Figure4.2: Optical attenuation coefficient and corresponding optical penetration depth in silicon as function of wavelength……………………………………………...….50

Figure4.3: Sketch of various light-trapping schemes………………………………….....51

Figure4.4: Images of black silicon structure (left), laser drilled texture………………….……54

Figure4.5: Patch texture (left, center). Diffractive dimple structure (right)…………….……...…55

Figure4.6: Sketch of the patch texture (left). Indicated by the white arrow is the function of the texture. ……………………………………………………………….…………… 56

LIST OF ABBREVIATIONS

Abbreviation	Meaning
AM1.5	Air Mass 1.5. Standard solar spectrum for solar cell efficiency measurements
ARC	Anti-reflection coating
AFM	Atomic Force Microscopy
DLTS	Deep-level transient spectroscopy
DOE	Diffractive Optical Element
FTIR	Fourier-Transform Infrared Spectroscopy
FCA	Free-carrier absorption
FWHM	Full Width Half Maximum
IR	Infra-red
IFE	Institute for Energy Technology
LCP	Laser Chemical Processing
LFC	Laser fired contacts
LIPSS	Laser Induced Periodic Surface Structures
HNA	Mix containing Hydrofluoric acid, Nitric Acid, Acetic Acid
MFD	Mode Field Diameter
OPO	Optical parametric oscillator
PL	Photoluminescence imaging
PV	Photovoltaic energy
PECVD	Plasma-Enhanced Chemical Vapor Deposition
QSSPC	Quasi-steady state photoconductance decay
RIE	Reactive Ion Etching
SEM	Scanning Electron Microscopy
SHG	Second Harmonic Generation
SRV	Surface recombination Velocity
THG	Third Harmonic Generation
TEM	Transmission Electron Microscopy
UV	Ultra-violet

ACKNOWLEDGEMENT

Given at any working environment a thesis in B.Sc.Engg. is definitely not a single man job. Proper team work under the inspiration of a great personnel is the least thing required for coming up with something good which may be economic for the world as well as efficient. We four Md. Nahid Hasan, Md. Abdullah Al Asif, Md Neazul Hasan and Md. Tanbin Rahman did try our best to do the thesis in a way that can possibly help the local government if not the whole world.

Firstly, we would like to thank our supervisor **Prof. Dr. Md. Ashraful Haque** who gave us the license to play in the field of solar thermal energy. Without his help and perfect guidelines the thesis would never be possible which would be a great loss for us. In fact showing any gratitude to him at this point would be less in any taken parameter.

Working with solar cell by applying laser processing required a lot of theoretical knowledge as we didn't have enough time to find them practically. In modern age we couldn't ask more from the internet and the reference papers we have used. For finding the most efficient way of photovoltaic silicon solar cell with laser processing, we had to depend on theoretical outcomes only and it left a great desire on us to work practically with it in upcoming days.
We four teammates felt so comfortable working with each other that made our thesis a better one from our expectation. We talked a lot, shared feelings, supported each other, and consoled each other when the results were not in our favor. That made something in our heart to work again with each other in our future life. Our work on light-trapping structures and laser processing technology would not have been the same without our cooperation with our supervisor. Your competence, patience and collaboration on this topic have been greatly appreciated.
We wish to thank our parents for being there, always interested when we talk about our work, and always supportive no matter what.

ABSTRACT

This thesis focuses on the use of lasers as a processing tool for silicon based PV. Lasers may perform a range of solar cell processes, such as edge isolation, doping, removal of dielectrics, structuring and contact formation, and have the potential to enable processes required for advanced, high efficiency solar cell concepts.

Solar energy is rapidly becoming one of the most promising renewable energy sources available to us. Its abundant availability greatly surpasses any other energy source, and with the immense progress seen in production technology for photovoltaics (PV) over the last decade, the price for converting solar energy into electricity is rapidly decreasing. However, further price reductions are still required for solar energy to be directly cost competitive with conventional energy sources in the majority of the world.

Two objectives were formulated for this thesis. The first objective focuses on acquiring new fundamental knowledge on the interaction between ultrashort pulse lasers and silicon and dielectrics used for solar cells. Such knowledge is valuable in itself, and is important for process understanding and development. The second objective focuses on the development of laser based techniques for the production of light-trapping textures. This as light trapping gets increasingly important as the wafer thickness used in industry is constantly being reduced and as new wafering techniques may render traditional texturing methods obsolete.

On the interaction between pulsed lasers and silicon or dielectric layers, emphasis has been put on ultrashort laser pulses. Mechanisms causing ablation and the process result after ablation have been the main focus. It has been shown that this plasma formation causes optical confinement of the laser energy which in silicon greatly reduces the optical penetration depth, and as such reduces the depth of the laser induced damage. Using lasers at a wavelength of 532 nm, the depth of the laser induced damage is reduced from approx. 3 µm to around 0.25 µm when going from nanosecond to picosecond pulse duration. Knowledge about the depth of laser damage as

function of pulse duration is valuable when seeking the right laser for a given process. In silicon nitrides, the plasma formation causes significant energy deposition into normally transparent films and may open for direct ablation of the dielectrics. It has also been shown that the ablation threshold on silicon is dependent on the temperature of the silicon substrate. In production, this would mean that the use of slightly elevated substrate temperatures would reduce the laser power required for a given throughput, or correspondingly increase throughput achievable with a given laser power.

On the topic of light-trapping structures fabricated by the use of lasers, two processes have been developed, and the performance of the textures has been measured. The patch texture, a geometric light-trapping texture for <100>-oriented monocrystalline silicon, showed a simulated increase in J_{cc} of 0.5 mA/cm^2 when compared with the random pyramids texture, being the current industry standard. New wafering techniques provide thin silicon wafers for which the patch and random pyramids textures may not be applicable, and for which no industry standard texturing process exists. With this in mind, a diffractive honeycomb texture was developed. The use of microspheres on the wafer surface as focusing elements enabled the production of features with sizes well below 1μm. The diffractive honeycomb texture shows a photo generated current of 38 mA/cm^2 on 21 μm thick silicon wafers.

The results summarized above shows that both fundamental understanding of the laser-material interaction and results that are directly applicable have come from the investigation of laser-material interaction. The texturing processes that have been developed show that laser based texturing processes are capable of delivering high quality textures suitable for a range of different substrates.

1 INTRODUCTION

Electricity from sunlight. Direct harvesting of the immense and never-ending power brought to us by the sun. Not long ago, this elegant way of generating electricity was associated with satellites and space stations, or remote off-grid locations needing electricity to power a light bulb in a cabin. Today, on the other hand, we can read that Germany generates 50 % of its electric power from photovoltaic (PV) energy during mid-day hours on a sunny day! In 2011, more than 28 GW of new PV generating capacity was installed globally. This corresponds to about 200 km^2 of solar panels, or 1.5 times the size of the city of San Francisco! Obviously, our view on PV as a small niche market needs to be reviewed.

In a world where a rapidly increasing demand for energy is ever more strongly conflicting with an urgent need to cut back on greenhouse gas emissions, it seems necessary and inevitable that renewable energy sources will play a major role in our future global energy system. A recent report from the Intergovernmental Panel on Climate Change predicts that wind and PV will account for up to 30 % of the world's electricity production by 2050, even in the moderate scenarios.

Direct solar energy is a tremendous energy resource, delivering around $4x10^{24}$ J of energy to the earth's surface per year (assuming a solar flux of 1 kW/m^2). The world's total energy consumption was in 2010 around $5.6x10^{20}$J, meaning that the solar energy hitting the earth in about one hour is sufficient to cover the energy needs of the humanity for a whole year! This is by far the biggest source of energy available to us, and a great candidate for a transition to a more sustainable energy system. Furthermore, silicon based PV is based on non-toxic, abundant materials, silicon being the second most abundant element in the earth's crust after oxygen.

PV is currently the fastest growing renewable energy source, with an average growth rate of above 40 % per year since the year 2000 (Figure 1.1). Silicon based solar cells have an 85 % market share, and is thereby the absolutely dominant technology in PV. The growth in PV has been linked to economic incentives, and continued growth in installed PV cannot rely on politically driven incentives alone. PV learning curves have, since the 1970's shown a 20 % reduction in module prices per doubling of cumulative production, a quite tremendous price reduction. This trend in price reductions however, has

to be continued as incentives are continuously being reduced. This can either happen through reduction of production costs (fewer $ per solar cell), or by an increase in efficiency (more watts per solar cell). A combination of both would of course be ideal. In the current situation, the price for manufacturing of the solar cell and solar module has been dramatically reduced. This leads to a situation where balance of system costs, such as installation costs, the costs of mounting brackets, land usage costs etc. are beginning to dominate the total cost of a PV energy system. Increased efficiency of the solar cell will reduce balance of system costs, e.g. by reducing the number of brackets and land area required for a given output power, meaning that retaining or improving the efficiency of the solar cell is essential for reduction of PV system costs.

The strive towards low cost, high efficiency solar cells has led to the introduction of several new processing tools and techniques that have enabled the impressive cost reductions seen in the PV industry. One group of tools that has the potential to change existing production techniques, and enable new processes and even new solar cell designs are lasers. Lasers have the ability to structure, cut or remove materials, alter the chemical composition of materials through the introduction of impurities, and several other processes. As shall be shown later in this thesis, there exists a range of solar cell related processes for which lasers can be applied. This thesis will focus on the use of lasers as a processing tool for improvement of silicon PV, where lasers have the potential to improve the efficiency of the solar cell and to reduce production costs.

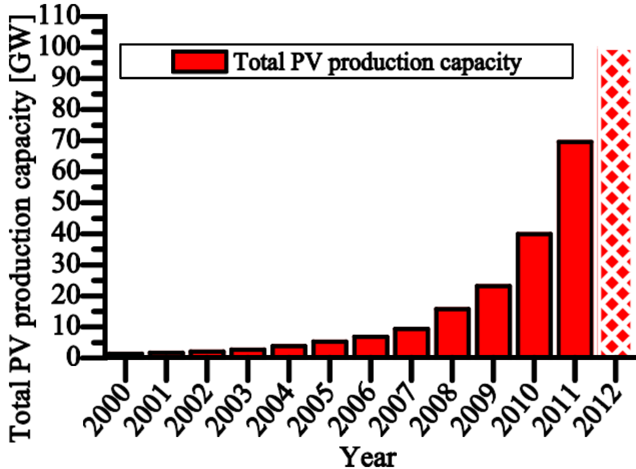

Figure 1.1: Total installed PV production capacity.

1.1 SILICON SOLAR CELLS

Solar cells operate by converting sunlight into electricity. In this section a brief review of the solar cell physics will be given. For a more thorough introduction.

One of the critical properties that make silicon suitable as a solar cell material is that it is a semiconductor, possessing a band-gap. This band-gap is a range of energies that the electrons in the materials are not allowed to have. The electron can either have an energy placing it in its ground energy state in the valence band, or it can be in an excited state in the conduction band. The electron can transition from valence band to conduction band and back through excitation and recombination processes described below. The energy required for an excitation may come from a photon, being the smallest package of energy one can divide light into. The sunlight consists of photons with a wide range of energies. The energy of the photon corresponds to what we observe as the color of the light, where the blue light consists of photons with a higher energy, and the red light consists of photons with lower energy. The energy of the photon also corresponds to a wavelength of the light, where the blue light has a shorter wavelength, and the red light has a longer wavelength. The spectral energy distribution of the sunlight is shown in Figure 1.3, adding up to 1000 W/m^2 at the earth's surface under given conditions, in what is known as the Air Mass 1.5 spectrum (AM1.5).

When a photon hits the silicon, it may be absorbed by an electron in the silicon, providing enough energy for the electron to be excited from its ground energy state in the valence band to an excited state in the conduction band, as indicated in Figure 1.2 a). Such an absorption process may only take place if the photon carries an energy corresponding to at least the band gap energy. The electron being excited will leave behind a hole in the valence band; an electron-hole pair is created. In a solar cell, the electron-hole pair moves by diffusion until it reaches the p-n junction. The p-n junction is a built-in asymmetry in the solar cell, where an electric field ensures that the electron will travel in one direction, while the hole travels in the opposite direction. As such, the electron may reach one of the electrical contacts, while the hole reaches the other contact, as a result of a combination of random diffusion and directional drift in an electric field. This is the principal mechanism for current generation in a solar cell. Only photons with high enough energy may be absorbed by the electrons. A photon with energy lower than the band-gap energy will not carry sufficient energy to lift the electron to the conduction band, and will as such not be absorbed in the semiconductor. Hence, its energy will not be converted into electricity.

This situation is indicated in Figure 1.2b), and is called sub-bandgap loss. On the other hand, photons with high energy can create an electron-hole pair as indicated in Figure 1.2 c), lifting the electron high above the conduction band edge. However, all the excess energy that is put into the electron will be rapidly lost, as the electron will collide with other electrons or atoms, losing energy until it reaches the conduction band edge. This loss process is called thermalisation.

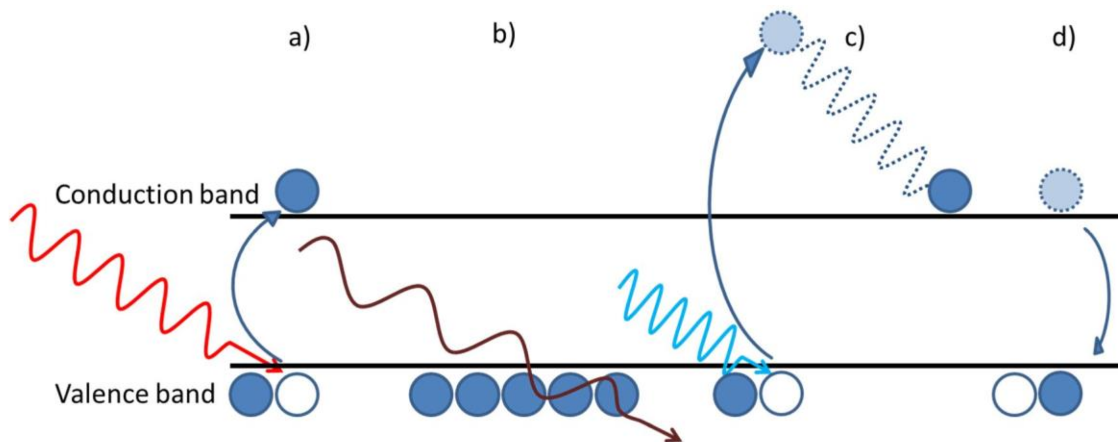

Figure 1.2: Illustration of some absorption and loss mechanisms in a solar cell. a) Absorption, b) photon with insufficient energy for absorption, c) absorption and thermalisation, d) recombination.

Figure 1.3 shows the spectral energy distribution from the sun as function of the wavelength of light. The area below the top graph indicates the total incoming solar energy, while the area below the lower graph indicates the energy available to us when taking into account the loss contributions discussed above, with a collective term called spectrum loss. Spectrum loss is a function of the band-gap energy of the semiconductor, and limits the efficiency of a silicon solar cell to below 50 %.

In a real solar cell, not all generated electron-hole pairs will contribute to current generation. There is always the chance that an electron finds a hole on its way to the contacts and relaxes back across the band gap, in a process called recombination, indicated in Figure 1.2 d).

Recombination may happen slowly in the bulk of a high-quality silicon wafer, but it will always take place even in a perfect material. These unavoidable recombination mechanisms are termed intrinsic recombination mechanisms. In a more realistic material, recombination happens faster. Examples of recombination-active areas are crystal defects or impurities in the silicon, highly doped silicon, silicon crystal boundaries or wafer surfaces and metal-silicon interfaces, such as contacts. By combining intrinsic recombination mechanisms with spectrum losses, we reach a maximum efficiency of a

solar cell, known as the Shockley-Queisser limit, which for silicon under an irradiance corresponding to the AM1.5 spectrum is around 29 %. Currently, the record efficiency of a silicon solar cell is 25 %, which is actually quite close to the theoretical maximum of 29 % given by the Shockley-Queisser limit.

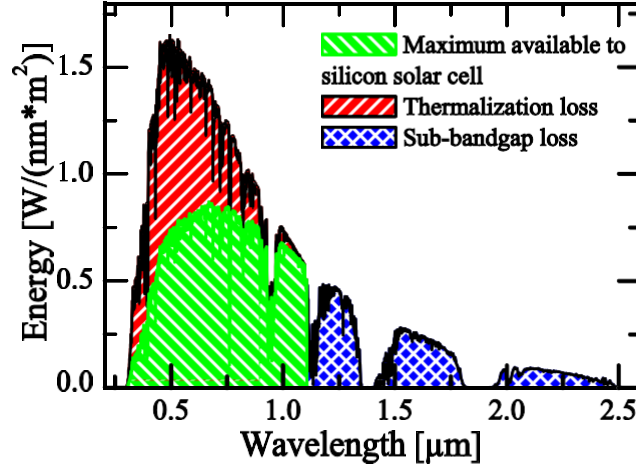

Figure 1.3: Solar irradiance (upper, black curve) and the maximum available energy to a silicon solar cell when considering spectrum losses.

The efficiency of the solar cell, 5 is of course of outmost importance. Several factors determine this cell efficiency which can be collected into the expression.

$$\eta = P_{CELL} / I_{SOLAR} = J_{SC} V_{OC} FF / I_{SOLAR} = J_{MPP} V_{MPP} / I_{SOLAR} \quad 1.1$$

In this expression, P_{CELL} is the output power density of the cell, I_{SOLAR} is the solar irradiance J_{SC} is the current density at short circuit conditions, being the maximum current available from a solar cell. V_{OC} is the voltage at open circuit conditions, being the maximum voltage available from a solar cell. As both open and short circuit conditions would lead to zero power output of the solar cell, the maximum power output of the solar cell is found by operating the solar cell at a voltage somewhat lower than V_{OC}, in what we call the maximum power point. J_{MPP} and V_{MPP} are current density and voltage at maximum power point, respectively, and the fill factor FF is the ratio of $J_{MPP}V_{MPP}$ to $J_{SC}V_{OC}$. We see from the expression that J_{SC}, V_{OC} and FF should be as high as possible.

1.2 MOTIVATION AND OBJECTIVE OF THE THESIS

The record silicon solar cell with an efficiency of 25 % mentioned earlier is a beautiful example of solar cell engineering. The problem, however, is that in order to make such a cell, several processes that cannot be directly transferred into mass production are employed. A common feature of several high-efficiency solar cell concepts is that they require some form of local processing, which on lab-scale cells has been enabled by photolithography. Photolithography is, however, generally considered incompatible with the very high throughput required by the solar cell industry. As lasers provide excellent spatial resolution and translational control, they may provide similar local processing capabilities with much simpler processes, and may as such open for industrial scale local processing and high solar cell efficiencies in industrial production. Indeed, local laser processing is making its way into industrial production lines today. Laser processing may, however, only be successfully implemented if the process does not have a negative impact on the quality of the solar cell materials.

In order to develop low damage laser processes, fundamental insight into the physical interaction between the laser and the solar cell materials is absolutely crucial. Using pulsed laser sources, the laser-material interaction will depend on laser pulse duration, laser wavelength and material properties. Fundamental understanding of these dependencies will give understanding of the laser parameters required for successful laser processes. As such, knowledge about the dominating physical mechanisms involved in laser-material interaction will serve as a foundation for development of good laser processes, or even the other way around, serve as a pointer towards yet to be developed laser sources required for a given process. Fundamental knowledge about laser-material interaction would be useful also outside the field of silicon photovoltaics. As such, the first main objective of this thesis is:

To gain fundamental understanding of the interaction between pulsed lasers and materials relevant for silicon solar cells.

The materials in focus shall be silicon and dielectric layers covering the silicon, functioning as e.g. anti-reflection coatings, passivation layers or diffusion or etch barriers.

The main focus shall be on parameter ranges giving material removal, called ablation, as ablation is required for a wide range of laser processes. This understanding shall be sought through a combination of experimental techniques and simulations. Laser sources with varying wavelength and pulse duration shall be applied on a selection of materials. Simulation models accounting for the physics encountered with the use of long (nanosecond) and ultrashort (picosecond) pulses shall be developed.

The second main topic of the thesis concerns thin silicon wafers. Silicon is an indirect band-gap semiconductor meaning that photons may travel quite a distance in silicon before they are absorbed. Thicker wafers would thus increase light absorption. Unfortunately, silicon is quite expensive, meaning that thick cells would be too costly. Currently, there is a strong drive in the industry to reduce the standard wafer thickness from the thickness used today (around 160 µm) to 120 µm by 2020. Today, wafers are typically manufactured by wire sawing, and almost half of the silicon is lost as “saw dust”, or kerf loss. Several novel techniques are being developed in order to eliminate kerf loss and enable production of even thinner wafers, between 20 and 50 µm thick, thus drastically reducing silicon consumption. With this trend in mind, development of highly efficient light-trapping techniques for efficient collection of the sunlight is needed. For these new kerf-less wafers, traditional texturing methods may not be applicable, due to e.g.
(i) the crystal orientation of the wafer or (ii) the lack of saw damage on the silicon surface for seeding of the structures or (iii) simply because currently available texturing processes remove too much of the silicon. Several approaches have been suggested, but a solution suitable for mass production is yet to be developed. The use of lasers for texturing of silicon wafers is interesting, due to the laser’s ability to create precisely defined geometrical patterns on the wafer surface. The use of a highly accurate laboratory laser setup would identify the practical limits to the texture quality achievable by laser based texturing. The second main objective for this thesis is

To develop laser-based techniques for manufacturing of efficient light-trapping textures.

The focus shall be on textures investigated theoretically in the literature, but for which no industry standard method exists. As laser-based texturing is not yet a mature technique,

emphasis shall be put on investigation of the achievable quality of the developed textures and their practical, rather than theoretical light-trapping potential.

1.3 STRUCTURE OF THE THESIS

This thesis is written as a collection of papers with an introductory text. The findings already presented in the papers will not be repeated to any length in the main text. The purpose of the main text is to provide an introduction to the field of solar cell research, motivate the topic of the thesis, and provide additional theory and experimental details that are not presented in the papers. The papers are appended at the end of the thesis.

The thesis is divided into 6 chapters. In chapter 1, the thesis is placed in a broader context and an introduction to solar cell technology is provided. At the end of the chapter, a summary of the articles is given.

Chapter 2 presents details of the main experimental tools and techniques utilized during the work with this thesis.

Chapter 3 is dedicated to laser-material interaction and laser damage. The chapter begins with an overview of the state of the art of laser processing for silicon solar cells. Then, laser-material interaction and the difference between long and ultrashort pulses are presented, followed by details on the simulation models applied within the thesis. Additional simulation results and physical insights that are not included in the papers are also presented in this chapter, and some methods for characterization of laser-induced damage are summarized.

Chapter 4 is dedicated to the subject of light trapping in silicon solar cells. The need for light-trapping structures is motivated, and some typical structures are presented. Some previously investigated methods for laser assisted structuring of silicon are reviewed, and the approach to laser assisted structuring chosen in this thesis is motivated. The industrial feasibility and potential of the processes is discussed, comparing the structures to industry standard methods.

Chapters 5 and 6 provide conclusions and suggestions on further work related to the investigation of laser-induced damage, investigation of laser-material interaction and further development of the light-trapping structures presented in the thesis

2 EXPERIMENTAL TOOLS AND TECHNIQUES

In this thesis, a number of experimental tools and techniques have been applied. Silicon wafers must be cleaned and prepared for processing. Often, a dielectric coating has been deposited onto the wafer surface. The laser has been the primary process tool, often accompanied by wet chemical etching. For characterization of the process result, a range of optical characterization techniques such as spectroscopy and microscopy have been applied. Also the electrical properties of the samples have been characterized. This chapter presents an overview of the main experimental tools and techniques applied during this thesis.

2.1 LASERS

The laser is the most important processing tool in this thesis. To two laser systems have been available at the Department for Solar Energy (IFE), and other lasers have been applied at other locations. These will be described below. The laser parameters are summarized in Table 1.

Green nanosecond laser
The affordable workhorse laser for silicon processing is the green nanosecond laser, more specifically, the frequency doubled diode-pumped solid-state (DPSS) laser. A Rofin Power Line 20 E – LP SHG2 laser has been available at IFE. It operates at 532 nm, with a pulse duration between approx. 50 and 250 ns.

Other solid state lasers
At the Laser Zentrum Hannover, experiments have been performed using solid state lasers with nanosecond pulse duration with a wavelength of 266 and 355 nm and 10-40 ns pulse

duration (Coherent AVIA) and 1064 nm and 30 ns pulse duration (IPG YLPM-1-A4-20-20).

Short pulsed CO_2-laser
A short pulsed CO_2-laser from a commercial supplier was applied. The laser pulse duration was approx. 100 ns, and the wavelength was 9.3 µm.

Ultrashort-pulse laser
For the majority of the work in this thesis, an Amplitude Systems-Pulse HP laser was applied. This laser has a second harmonic – third harmonic generation (SHG – THG) module. The laser itself delivers pulses that by an adjustable pulse compressor can be freely selected to values between approx. 0.5 ps and 6.5 ps at a fundamental wavelength of 1030 nm. Second and third harmonic wavelengths of 515 and 343 nm are available by adjusting the power through the SHG – THG module. The laser is equipped with both a galvo scanner and fixed lenses, and a xyz-table for sample translation. For the processing in PAPER IV, a top-hat beam shaping element from Eksma Optics was applied. This element transforms a Gaussian beam profile into a uniform, square intensity distribution. Such an intensity distribution allows for uniform processing of larger areas, but the output intensity distribution is sensitive to the exact beam shape and quality of the incoming beam.

Table 1: Summary of laser parameters.

Laser model Parameter	Oxford Laser/ Amplitude s-pulse HP	Rofin Power Line LP	Other nanosecond lasers
Wavelength [nm]	343, 515 and 1030	532	266,355, 1064 and 9300
Pulse duration [s]	$0.5-6.5\times10^{-12}$	$50-250\times10^{-9}$	$10-100\times10^{-9}$
Repetition rate [kHz]	1-300	10-100	
Beam diameter in focus [µm]	9-40	40	
Beam quality (M^2)	<1.3	<1.3	<1.4

For the majority of the work within this thesis, non-overlapping laser pulses are utilized, as incubation effects are observed where multiple pulses are applied. Slight surface and volume modifications from previous pulses will increase absorption, thereby reducing the ablation threshold and cause the formation of larger surface structures (ultimately providing black silicon,) that are undesirable when investigating the topics of this thesis. Two types of incubation effects are shown in Figure 2.1, using ultrashort laser pulses. (Top left) SEM image of self-assembling structures similar to those found in so- called black silicon, developed by irradiating one spot with multiple pulses. (Top right) SEM image of laser-induced periodic surface structures (LIPSS). LIPSS are periodic waves or ridges with size on the order of the wavelength of the applied light, developed by applying partially overlapping pulses. (Bottom left) AFM height profile of LIPSS. (Bottom right) Area covered with LIPSS viewed at different angles. Different viewing angles gives different wavelength, characteristic for diffraction.

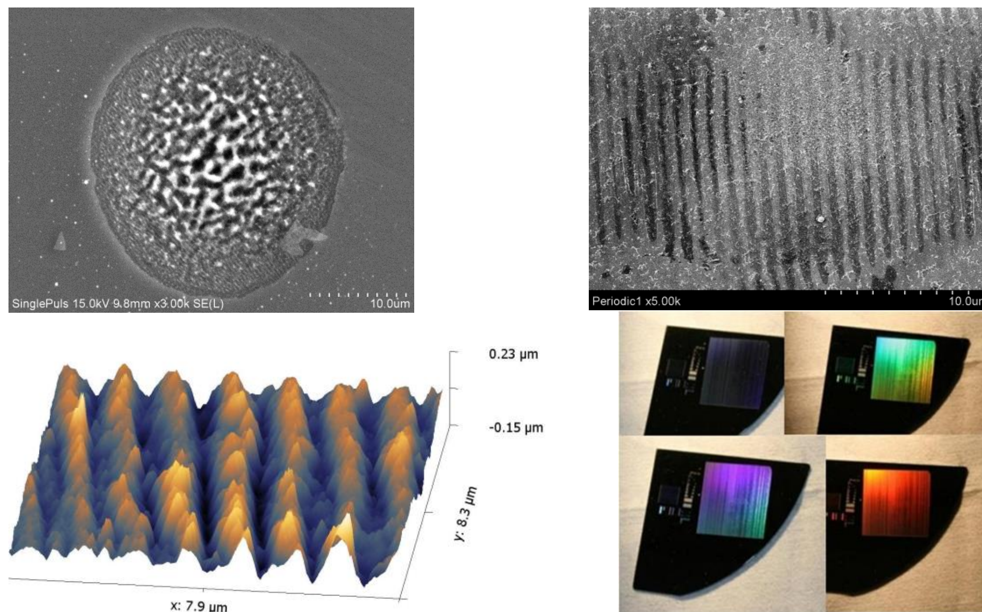

Figure 2.1: Surface modifications caused by ultrashort laser pulses. Top left: SEM image of multiple pulse irradiation in one spot, causing surface structures to appear. Top right: SEM image of Laser-induced periodic surface structures (LIPSS). Bottom left: AFM height map of the same LIPSS structure. Bottom right: Wafer with LIPSS photographed at different angles, showing the typical rainbow-appearance characteristic of diffractive surfaces.

2.2 EXTRACTION OF LASER PARAMETERS

As stated above, non-overlapping pulses were applied during the majority of the work with this thesis. Processing with these conditions normally gives a region on the wafer surface that has in some way been affected, and the extension of the affected area will depend on a

range of laser and process parameters. The process most frequently investigated in this thesis is the ablation of dielectrics from a wafer surface, and the ablated diameter is often sought. Examples of spots with a clearly defined ablated diameter are seen in Figure 2.1 (Top left) and Figure 2.2.

The laser ablation process is often characterized by the laser fluence required for ablation to take place, known as the ablation threshold fluence (ablation threshold) F_{th}. This quantity is of outmost importance when describing the ablation process, and is generally dependent on material parameters and laser parameters such as laser wavelength and pulse duration. While the wavelength is set directly by the laser, the pulse duration and laser fluence must be measured or controlled externally.

The laser fluence is only available to us indirectly, by measuring several quantities, these being average laser power, pulse repetition rate and spatial fluence distribution. The average laser power was measured using a PS19Q thermopile power sensor from Coherent Inc. This sensor has a rated sensitivity of 10 μW, and a calibration accuracy of 1 %. Practically, however, the measured power tends to fluctuate more than this, especially at low powers, as a result of power sensor inaccuracies or as a result of actual variations in laser output power. Therefore, 5 % has been used as the uncertainty of the laser power meter.

The spatial fluence profile of a laser beam may be quantified by its M^2 – number, where $M^2 = 1$ describes a Gaussian fluence distribution. This distribution is also the one where the tightest focus is obtainable. All other fluence distributions have an $M^2 > 1$, and as such have larger foci by a factor of M^2. The lasers applied in this thesis are nearly Gaussian, showing an M^2-value of below 1.3. As such, the fluence profile is assumed to be Gaussian. However, also the width of the Gaussian fluence distribution must be known, which will vary depending on how far from the focal plane the sample to be processed is located. Liu describes a method for extracting the beam diameter of a Gaussian beam by measuring the diameter of the ablated area as function of pulse energy. The method also gives the ablation threshold fluence, and is as such a valuable tool in characterization of laser ablation, and is described by the expression:

$$(R_{ABL})^2 = (c^2/2)\ln(F_0/F_{th}) = (c^2/2)[\ln(2E/\pi c^2) - (\ln F_{th})] \qquad 2.1$$

Here, R_{ABL} is the ablated radius, c is the beam radius measured at the point where the intensity has dropped to $1/e^2$ of the peak fluence level. F_0 and F_{th} are the peak fluence

of the laser pulse and the ablation threshold fluence. Using the right hand side expression, requires only the ablated radius r and pulse energy E, which both can be measured, and the unknown quantities, namely F_{th} and c , that are found by fitting the expression to the measurement data.

The ablated diameter has been found using the image processing program ImageJ, by using the color contrast between the ablated spot and the remaining dielectric layer, as shown in Figure 2.2. One challenge using this technique is that the color change seldom is step-like. There will always be a blurry area where the color is in between that of the spot and the surroundings and was found in combination with uncertainty in the power meter and deviations from the modeled trend to be around +/- 20 %. It is also seen in Figure 2.2 that the spot is not perfectly round. The ablated radius, R_{ABL}, is estimated from the ablated area, A_{ABL} through

the relation $R_{ABL} = \sqrt{A_{ABL}/n}$.

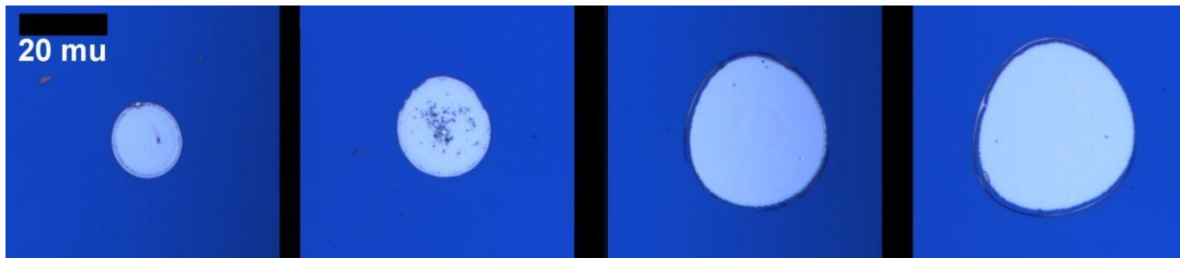

Figure 2.2: Typical set of images used as data for the method by Liu. Shown here is the ablated spot obtained when ablating SiN_x from Si using a laser wavelength of 1030 nm and a pulse duration of 3 ps. The applied laser pulse energy increases from left to right.

The pulse duration was only measured for the ultrashort pulses, at the fundamental wavelength using a Pulse Check 50 auto correlator from APE (Angewandte Physik & Elektronik GmbH). The pulse duration at second and third harmonic wavelengths were not directly measured, as the auto correlator was not built for these wavelengths. The pulse duration at harmonic wavelengths may be shorter than at the fundamental wavelength, as a result of the intensity dependence of the efficiency of the wavelength conversion process, or longer, as a result of dispersion effects. The manufacturer has measured the pulse duration at the second harmonic wavelength, finding that this pulse duration approximately equals that of the fundamental wavelength, possibly being marginally shorter. The laser manufacturer expects the same behavior at the third harmonic wavelength. In this work, it is assumed that the second and third harmonic pulse have the same pulse duration as the fundamental wavelength pulse.

2.3 THIN FILM DEPOSITION

In solar cell processing, thin dielectric films are frequently deposited onto the silicon wafer in order to improve optical or electrical properties. The typical blue color of a solar cell arises from a thin anti-reflection coating, reducing the reflectivity of the solar cell. Other films may primarily be deposited in order to reduce recombination at the wafer surfaces.

The dielectrics used in this work (with the exception of one thermal oxide) were all deposited by plasma-enhanced chemical vapor deposition (PECVD), a technique commonly used for dielectric deposition in the PV industry. In the PECVD process, reaction gases are ionized by an electric field, in the PECVD system applied in this thesis an RF field. This ionization helps improving the reaction rate and allows for fast deposition at relatively low temperatures. An Oxford Instruments Plasmalab System 133 PECVD system was used for this deposition. For laser processing, silicon nitride (SiN_x) has been most frequently used, but also some silicon oxide (SiO_x) and silicon ox nitride (SiO_xN_y) films. For passivation, amorphous silicon (a-Si) was used in order to obtain very low surface recombination velocity. Generally, all films deposited by PECVD will contain relatively large amounts of hydrogen, and the films deposited in this thesis are amorphous. As such, a more precise description of the films would be e.g. hydrogenated amorphous silicon nitride (a-SiN_x: H), but for convenience, the shorter notation given above shall be used. Here, several different SiN_x films were deposited. The composition of these films was varied by adjusting the flow of silane (SiH_4) to the chamber, while keeping all other deposition parameters (gas flows, pressure and temperature) constant.

The surface-near damage to the silicon is observed after deposition of PECVD SiN_x, observed in the form of reduced lifetime on samples where the SiN_x was removed in a 5 % hydrofluoric acid solution and the wafer was subsequently passivated with a-Si. As this damage was discovered late in the thesis, there was no time for more thorough investigation of the damage mechanisms, and the damage is tentatively attributed to ion bombardment from the deposition process.

2.4 MICROSCOPY

Both in the work with texturing processes and in the work on laser – material interaction, microscopy has been used extensively for measurements on ablated diameters and general

quality of process assessments. For this work, a Zeiss Axioskop 2 MAT optical microscope was used.

A Hitachi S-480 scanning electron microscope (SEM) has been applied for more detailed analysis. The SEM has very high depth of view and high resolution, and is as such well suited for the investigation of textured surfaces and small features. Bare silicon or silicon with a partial dielectric cover have been investigated in the SEM. The limited electrical conductivity of these samples has in some cases limited the resolution and contrast of the SEM images, but has the advantage that the process result is not covered up, as would be the case if coating the sample with a conductor before performing SEM.

For accurate height-profiles on the nano-scale, a Pico Station atomic force microscope (AFM) from Surface Imaging Systems has been applied. This AFM was not equipped with a microscope, and hence, searching across the sample was a tedious task. Furthermore, scanning as large as 47x47 µm requires rather large scan speeds, on the order of 10 µm/s. This results in vulnerability to loss of accuracy, especially when encountering debris on the surface. The open-source program Gwyddion was used for post- processing of the images. As most AFM images show bow or tilt, a polynomial background (2nd order) was removed by masking out the laser spot and assuming that the wafer surface outside of the laser spots was flat. However, the leveling may not be completely accurate. As such, the line profiles may still carry some artifacts due to bow or tilt that hasn't been completely removed, ablation craters from the ablation of SiN_x are analyzed, showing height differences of a couple of tens of nanometers over a couple of tens of micrometers. Such slow height variations will be sensitive to residual bow, and the measured height differences should be treated with caution. These distortions are not expected to be critical to the analysis of the profiles, as e.g. step-like height profiles are still clearly visible.

2.5 WET CHEMICAL PROCESSING

Several different wet chemical processes have been applied in this thesis, either for cleaning or for structuring or removal of the silicon. These will be briefly summarized here.

Cleaning

All samples were dipped in a 5 % hydrofluoric acid (HF) solution for 1 minute before thin film deposition. This removes any oxide layer on the wafer surface. HF was also used after laser processing in the cases where remaining SiN_x or SiO_x needed to be removed, specifically if the wafer was to be passivated or the whole surface was to be etched.

Samples intended for lifetime measurements were in addition etched in a piranha solution (4:1 sulfuric acid: hydrogen peroxide, (4:1 H_2SO_4:H_2O_2)) and in concentrated hydrochloric acid (HCl), in order to ensure the best possible surface passivation. Piranha removes organic residues, while HCl removes metallic contaminations. These etches remove no or only very little silicon, and as the surface-near laser damage is sought, this processing will not influence the sought-after results.

Silicon etches

Three silicon etches have been applied in this thesis. Firstly, for the creation of the patch textures, a 10 % potassium hydroxide (KOH) solution at 88 °C was applied. Low concentration KOH solutions preferentially creates pyramidal structures by exposing <111> crystal planes. Increasing the concentration of KOH from 2 to 10 % ensured a more practical etch time reaching a depth of 10 µm in less than 10 minutes. Figure 2.3 (top left) shows an inverted pyramid structure which is not fully formed, as a result of too short etch time, and complete inverted pyramids by increasing etch time (top right).

For the etch-back experiments, flat surfaces are desired, and a homogenous etch is preferred. For this purpose, a 47 % KOH solution at 88 °C was used, as high concentration KOH solutions tend to leave behind a rather flat wafer surface. An example of a wire-sawn wafer etched in high concentration KOH is shown in Figure 2.3 (bottom left). The samples applied in this thesis are polished, and the result of high concentration KOH etching is very flat as shown in Figure 2.3 (bottom right). The high concentration KOH etch showed an etch rate of approx. 1 µm/min, and it was as such easy to achieve relatively shallow etches. Both KOH etches were kept in a water-bath for better temperature control.

An isotropic etch was required. An HNA (Hydrofluoric acid, Nitric acid, Acetic acid) etch was chosen. As described, the processing results were improved when increasing the HF content in the HNA solution from 1:40:15 to 5:40:15, as under-etching was suppressed. It is suspected that under-etching is caused by a mechanism allowing the acid to penetrate more rapidly along the wafer surface, thereby increasing the area of attack of the etch.

Such mechanisms could be either an interface oxide layer, as silicon oxide has a high etch rate in this solution, or surface-near crystal damage. Damaged crystals may have more attack points for the etch, and may as such have a higher etch rate than an undamaged crystal.

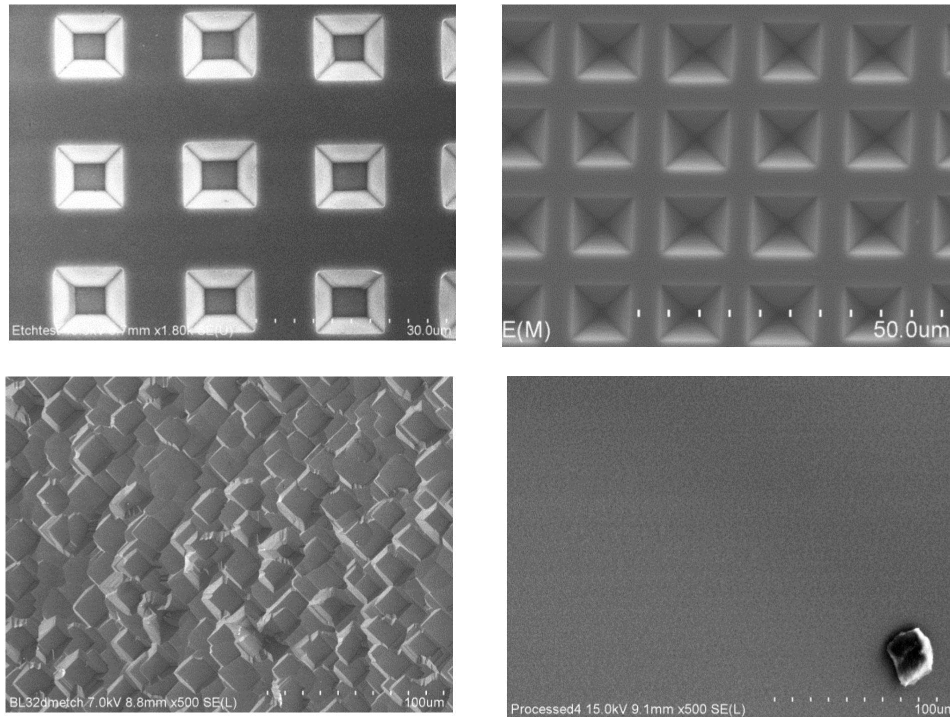

Figure 2.3: (Top) Inverted pyramid structure showing incomplete (left) and complete (right) etching. (Bottom) KOH polishing etch on slurry-sawn wafer (left) and on polished wafer (right). No structures are observed on the polished wafer, an image with a piece of debris in the lower right corner is chosen in order to indicate the image resolution and contrast.

2.6 REFLECTANCE AND TRANSMITTANCE MEASUREMENTS

For several of the experiments in this thesis, optical quantities must be characterized. For experiments on laser – material interaction, the reflectance gives information about the amount of laser energy entering the silicon. Reflectance for these samples was measured using a spectrometer-based setup from Ocean Optics, using an integrating sphere in a one-port setup. Such a setup will introduce a substitution error when the calibration sample has a different reflectance than the sample to be characterized, the substitution error increasing with increasing difference between the reflectance of the calibration sample and that of the measurement sample. For these measurements, polished silicon was used as reference

sample, ensuring that the absolute error when measuring a reflectivity around 5 – 15 % is well below 1 %. As the reflectivity in the case of laser-material interaction experiments only influences the intensity entering the silicon by a small amount, this substitution error is acceptable, and much lower than e.g. the uncertainty in the method by Liu, described in section 2.2.

For measurements on light-trapping structures, on the other hand, greater accuracy is required. For the geometric light-trapping structures, the same spectrometer-based setup was used, but the integrating sphere was replaced with a two-port sphere. This sphere allows for the calibration sample to be mounted at one port and the sample to be mounted at a second port, allowing the sphere as such to remain unchanged between calibration and measurement. This eliminates the substitution error described above.

The laser intensity dependence of the reflectance has also been estimated through rough measurements. As will be discussed in section 3.3.3, the dielectric response of a material containing a dense plasma of excited electrons may deviate from its steady-state value if the plasma contribution to the dielectric permittivity is considerable. In order to monitor this behavior, the reflectance was measured in-situ while laser processing. For these measurements, the sample was processed at 15° angle of incidence, and the reflected laser power was measured as function of incoming laser intensity using the thermopile power meter described above. This ratio gives the average reflectance. These measurements will be rough, as there is substantial uncertainty in the power measured with the power meter. Furthermore, the measured reflectance will be averaged both in time and over the whole area of the spot. Any diffusely reflected light will not be collected by the power meter. Still, there is a measurable trend towards higher reflectivity when increasing the optical intensity.

2.7 MINORITY CARRIER LIFETIME

In order to quantify the effect of laser induced damage, the effective minority carrier lifetime has been measured. Quasi-steady state photo conductance decay (QSSPC)

measurements have been applied, using a WTC-100 setup from Sinton instruments. This technique registers changes in conductivity of a sample under varying illumination, while at the same time measuring the illumination intensity. This gives information about how quickly the carriers decay in the wafer. Photoluminescence imaging (PL) has also been applied, using a LIS-R1 instrument from BT imaging. PL is a quick method for obtaining a spatially resolved lifetime map of a sample. This technique measures the photoluminescence signal from a wafer, and uses a QSSPC measurement to calibrate the relation between the photoluminescence signal and the minority carrier lifetime. The calibration measurement must be performed on a wafer or part of a wafer with relatively homogenous lifetime for good calibration accuracy.

Both of these measurement techniques measure the effective minority carrier lifetime. When measuring the lifetime of a laser processed sample, the inverse effective minority carrier lifetime can be expressed as the inverse sum of lifetime from various recombination mechanisms. Contributions may be divided into surface recombination, bulk recombination, recombination in the laser-damaged areas and any other relevant recombination mechanisms:

$$(1/\tau_{eff}) = (1/\tau_{surf}) + (1/\tau_{bulk}) + (1/\tau_{laser}) + \ldots\ldots\ldots\ldots\ldots$$

In order to isolate the effect of the laser processing, τ_{surf} and τ_{bulk} should be large. A large τ_{bulk} is ensured by using a high-quality substrate while a large τ_{laser} achieved by applying an efficient surface passivation. As described above, amorphous silicon was used for surface passivation as it gives excellent surface recombination properties.

2.8 SILICON SUBSTRATES

Throughout this thesis, polished silicon wafers have been applied. Hermann *et al.* have shown that laser processing of textured substrates may induce more damage than if processing on polished substrates, and as such, the transition to textured surfaces is not expected to be trivial. For the diffractive texture described in section 4.3.2, it may be difficult to spin the microspheres onto non-polished wafers. Also the passivation of rough surfaces may be more difficult than passivating polished surfaces. Still, the use of polished substrates is relevant, firstly, as trends and results may be clearer and easier to interpret,

and secondly, as several of the emerging kerf-less wafering technologies deliver substrates with surfaces that are close to polished in appearance.

3 LASER PROCESSING FOR SILICON SOLAR CELLS

This chapter provides a review of the state of laser processing for silicon solar cells. Thereafter, the theory behind laser-material interaction is discussed, and the simulation models are presented. Some of the results from these simulations are presented, along with some thoughts on laser interaction with a free-electron gas. Thereafter, the characterization and quantification of laser damage is discussed.

3.1 STATE OF LASER PROCESSING FOR SILICON SOLAR CELLS

In many cases, a laser being directed at a material is nothing but a source of energy or heat. The laser carries energy which may be absorbed by the material, thereby depositing energy into the material. Depending on how much energy is deposited, the material may be heated, melted or vaporized / ablated. This mechanism is the primary mechanism by which lasers may process a material or device.

Laser processing of silicon is not a new idea. In the late 1970's scientists were applying lasers to anneal damage from ion implantation. When annealing, the material, in this case silicon, is heated, normally by an infrared lamp, in order to increase the thermal energy of the atoms in the lattice. Thereby, defects, e.g. atoms that have been moved out of their regular place in the lattice, may diffuse back, restoring the regularity of the crystal. In laser annealing, the energy from the laser causes a controlled, localized heating of the wafer, and it was intended as an alternative to conventional thermal annealing.

For silicon solar cells, one of the primary motivations for applying lasers is the need for local processing, i.e. the need to process only a small part of a solar cell. Lasers show outstanding focusing, translational and temporal properties making them potent tools

for local processing. A range of laser-related processes for silicon solar cells have been developed, some of which will be briefly summarized below. Some of these processes and their influence on solar cell performance are indicated in Figure 3.1.

Laser edge isolation
In a solar cell process, one often obtains a cell where the diffused emitter is wrapped all the way from the front side of the cell to the rear side of the cell, thereby shunting the cell. This shunt must be removed, and lasers may be applied for the process. By removing the emitter by laser ablation around the edge of the solar cell, the shunt is effectively eliminated, and the fill factor, FF, is increased. This is shown in Figure 3.1 as a grove through the emitter at the edge of the solar cell. Laser edge isolation is currently implemented in industry.

Local contact openings
The metal-semiconductor interface shows a very high rate of electron-hole recombination, and is as such a significant source of efficiency loss in a solar cell. By applying local rear contacts instead of contacting the entire rear surface of a solar cell, recombination losses may be strongly reduced. Reduced recombination increases V_{OC}, and also J_{SC}, by increasing the fraction of the generated electron-hole pairs that reach the contacts. Local contacts may be created using lasers, simply by applying a laser to locally remove a passivating dielectric layer from the wafer surface, and metallize through these holes, shown in Figure 3.1. The main obstacle for successful implementation of this process is the laser induced damage to the silicon substrate. Locally contacted solar cell designs are on their way into industrial production, applying laser opening of the contacts.

Laser fired contacts
Laser fired contacts (LFC) is another method for creating local contact openings. In the LFC process, the silicon wafer is covered with a passivating dielectric layer, and the rear contact aluminum is deposited onto this dielectric. Contact with the silicon is created by irradiating this stack with a laser, whereby the aluminum, dielectric, silicon stack melts and the aluminum is forged into contact with the silicon. In this process, the silicon and aluminum are mixed, and aluminum diffuses into the silicon bulk. This creates a so- called back surface field, an electric field that will repel the electron from the recombinative metal-semiconductor surface, thereby strongly reducing recombination also in the metallized areas themselves. Industrial production equipment for LFCs is available.

Laser transferred contacts

One further way of creating metal contacts using lasers is the Laser transferred contacts or Laser induced forward transfer. In this method, a thin metal foil on a transparent carrier is kept close to the solar cell surface. A laser is irradiated through the transparent carrier, and the metal is ablated from its carrier, being deposited onto the solar cell.

Laser doping

Laser doping normally occurs through laser heating and melting of a silicon surface covered with a dopant-containing substance, whereby dopant atoms may be rapidly introduced into the silicon material, causing the silicon to become doped. Laser doping of silicon has been performed since the 1980's. Currently, laser doping is most relevant for the application of selective emitters, where doping is only performed on parts of the substrate, in order to form low resistance contacts, while allowing for a lighter emitter doping on the rest of the cell. Selective emitters thereby reduce series resistance, increasing FF , while reducing emitter recombination, thereby increasing J_{OC} . Several fabrication methods have been proposed. Firstly, doping from a solid state dopant source on the wafer surface may be applied. A spin-on dopant or the phosphorus glass from the emitter doping process may be used as dopant sources. Alternatively, laser chemical processing (LCP) has been proposed, in a method where the laser light is guided to the wafer in a jet of phosphoric acid, the acid serving both as a dopant source, light guide and cooling medium. Also laser transfer doping has been suggested. This is a process similar to laser transferred contacts, where doped amorphous silicon is transferred to the wafer. Selective emitters is shown in Figure 3.1 as a dark grey area under the front contacts. Selective emitters will allow for lower emitter doping on the rest of the wafer surface, thereby reducing recombination losses in the emitter, increasing the collection probability of the short-wavelength part of the sunlight, whereby increasing J_{cc} and V_{oc} . Industrial production equipment for selective emitters by laser processing is available.

Laser surface texturing

Surface texturing increases light-trapping, thereby increasing J_{OC}. Several approaches to surface texturing by the use of lasers have been reported. Ultrashort-pulse lasers may be applied for laser texturing. When a silicon substrate is irradiated by multiple ultrashort laser pulses, self-organizing structures begin to emerge. These often cone-like structures reduce the front surface reflectance of the solar cell, in what is often called black silicon

Alternatively, a macroscopic pattern may be drilled into the wafer, in a process where the laser does the material removal. A third option would be to use an etch mask that is opened locally using a laser, followed by etching through these holes. In this process, the etching does the material removal. Laser surface texturing shall be considered in more detail in chapter 4.

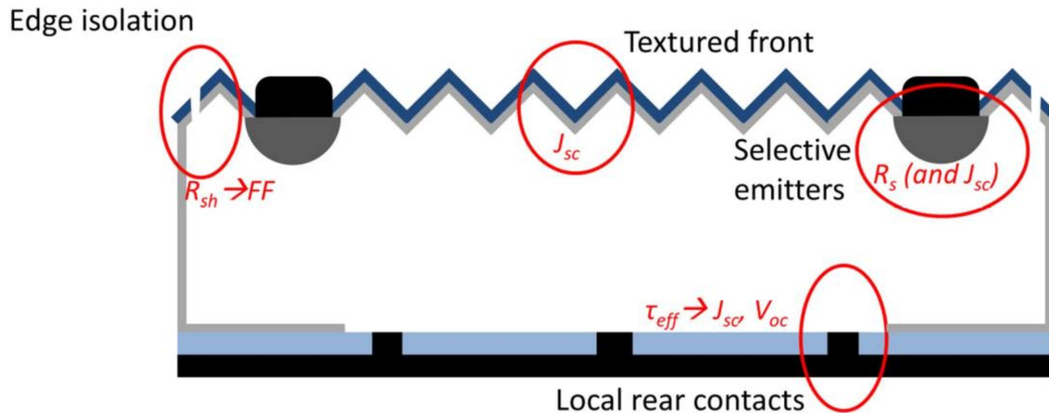

Figure 3.1: Schematic cross-section of a solar cell, highlighting potential areas for laser processing, and their influence on solar cell performance. The silicon wafer is shown in white, the emitter in light grey, local over- doping under the contacts in dark grey, anti-reflection coating in dark blue, rear surface passivation layer in light blue, contacts in black. Residual laser damage may be present in all laser processes.

Alternatives to laser processing

For the processes mentioned above, alternatives that do not apply lasers exist. Edge isolation may be performed by etching of the edges of the cell. Selective emitters may be formed e.g. by creating a thick emitter over the whole wafer surface followed by a masked etch, whereby the thick selective emitter is left under the contacts, while the emitter is thinned over the rest of the wafer, or by applying doping from locally printed dopant sources. Local contacts may be formed e.g. by dispensing the metallization paste in a pattern ensuring that the silicon-metal contact is formed only locally. Surface texturing is currently performed by wet-chemical etching, but also reactive ion etching (RIE) and microwave plasma etching may be applied. Laser processing is not automatically beneficial for the solar cell, as it may damage the quality of the solar cell materials, e.g. by introducing defects into the silicon, thereby increasing recombination, and decreasing V_{oc}. As such, laser processing is only relevant in cases where the laser process outperforms the alternative in terms of overall increase in cell efficiency, process simplicity, or cost.

From the overview given in this section, it is seen that the interaction between laser and material can give rise to a wide variety of processes. It is also seen that the damage to

the material resulting from the laser process must be under control for successful process implementation. As such, knowledge about the laser-material interaction is crucial, as is knowledge about the laser induced damage. The next sections are devoted to these topics.

3.2 LASER-MATERIAL INTERACTION

One of the main topics of this thesis is the laser-material interaction. The silicon, or a silicon–dielectric stack, is irradiated with laser pulses, and the laser light is absorbed. How and where this absorption takes place, combined with the properties of the irradiated materials and the laser parameters, such as pulse duration, laser wavelength and laser intensity distribution determines the outcome of the laser processing. In order to predict experimental trends or understand experimental results, it is relevant for us to understand the laser–material interaction in detail.

For the case of silicon, there is an observable change in processing results when reducing the laser pulse duration. A transition happens somewhere between nanosecond (“long”) and picosecond (“ultrashort”) pulse duration. Some typical process results when removing silicon nitride from silicon is seen in Figure 3.2, showing SEM images of processing with long and ultrashort laser pulses in the UV (343 / 355 nm), visible (515 / 532 nm) and infra-red (IR) (1030 / 1064 nm). The ultrashort pulse laser operates at the shorter wavelengths. Starting with long pulses in the visible wavelength range, the result is a molten area in the silicon, however, with relatively homogenous size. Long pulses have time to melt a significant amount of silicon, and re-distribution, i.e. pits and silicon expulsion is frequently observed. Looking at long pulses in the IR, the situation is somewhat similar, the melting is clearly visible. However, the pulse to pulse variation in processing result is much larger. This as a result of the inherent instability of the process. When cold, silicon is nearly transparent to this wavelength, with the laser light penetrating several hundred micrometers. However, some of the laser light is still absorbed. The silicon is slowly heated to the point where it absorbs strongly, whereby the deposited energy density strongly increases and enough energy is deposited to melt and vaporize the material. This feedback mechanism makes processing near the process threshold unstable, as the onset of absorption may depend on local material parameters. At shorter wavelengths, the picture changes. In the UV, the laser energy is absorbed by the SiN_x, decomposing this. However, the image shows an inhomogenous process result. This is an indication that some of the laser light penetrates to the silicon, with the possibility that the

silicon is vaporized and expels some of the SiN_x. Experiments have also been performed at 266 nm, where the SiN_x absorbs even stronger. Here, the instabilities observed when processing at 355 nm are not observed, as very little laser light will penetrate to the silicon. With ultrashort laser pulses, the picture changes somewhat. In the UV, the SiN_x still absorbs, but no instabilities are observed. Also in the visible and IR, the process results are, in general, much more homogenous. Furthermore, the obvious signs of melting and expulsion are gone, leaving a seemingly flat wafer surface. Whether using a pulse duration of 0.5 ps or 10 ps, the process results look similar when observed by SEM. Processing in the far-IR using long pulses gives process results resembling those observed with pulses in the IR, as similar heat-dependent feedback-mechanisms are dominant also here, and as the pulses are long enough for material expulsion and redistribution.

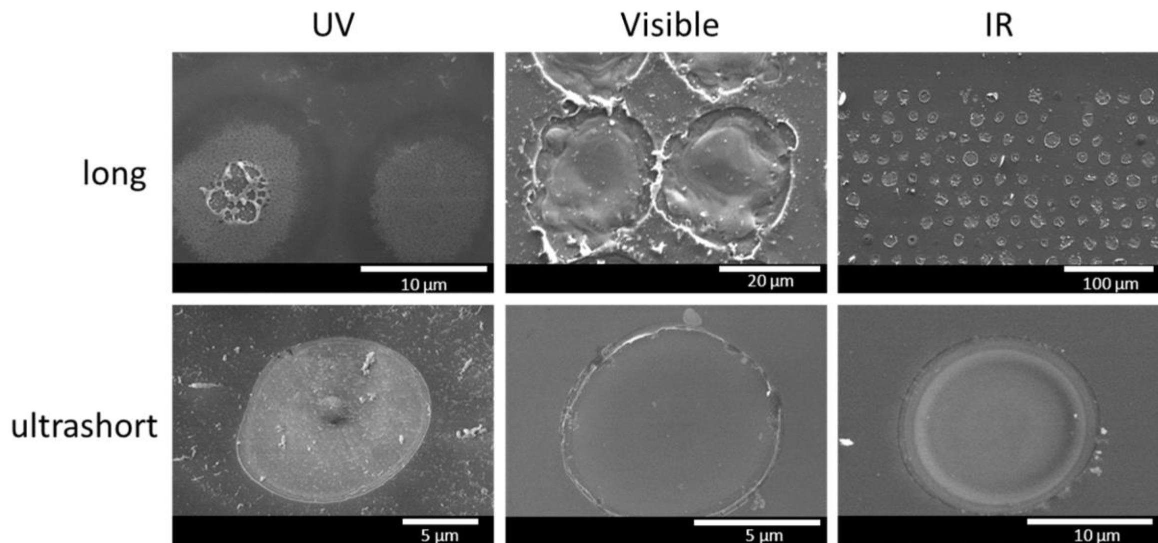

Figure 3.2: Typical process results when irradiating a silicon nitride on silicon stack with long and ultrashort laser pulses at 355 (UV), 532 (Visible) and 1064 nm (IR).

Above, it is stated that the laser light may be deposited into the SiN_x if the wavelength is short enough. Using ultrashort laser pulses, it can sometimes be rather straightforward to see where the energy has been deposited. Figure 3.2 shows that when processing in the UV using ultrashort laser pulses, the surface is covered in fine debris. In this case, the energy is deposited into the SiN_x, and the SiN_x is blown apart upon removal. This is in contrast to what is the case e.g. in the visible wavelength range, where the laser energy is deposited into the silicon. Here, it is frequently observed that the SiN_x which is blown off remains in one single piece that can be found elsewhere on the wafer upon inspection. This is shown in Figure 3.3.

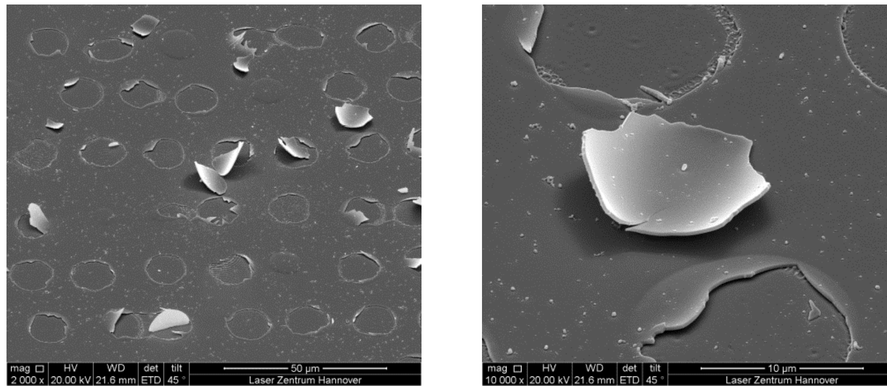

Figure 3.3: SEM images of complete pieces of SiN_x removed from the wafer surface using ultrashort pulses in the visible wavelength range. (Left: Overview, Right: close-up)

As the mechanism for ablation is different in these two situations, a distinction shall be made. The process where the laser energy is deposited in the substrate, and the film is lifted off by the vapor pressure substrate shall be referred to as indirect ablation. On the other hand, if the energy is deposited into the film, we shall refer to the process as direct ablation.

Not only has the appearance of the processing result changed when reducing the duration of the laser pulses. Also the physics of the interaction will change. Generally, the laser energy is absorbed by the electrons in the material, moving these to an excited state. When applying long laser pulses, this energy has time to dissipate to the lattice through collisions, whereby the electrons relax into less excited states. As such, there is equilibrium between the electron and lattice systems, the number density of excited electrons will remain moderate. There is also enough time for the heat to be transported a significant distance from where it is deposited.

This picture changes when going to ultrashort laser pulses. Now, the electrons will not have time to transfer their energy to the lattice before the pulse is through, and as such, the electrons may have significantly higher energy than the lattice during the pulse. Non-linear absorption may be encountered, meaning that the absorption is changing with the intensity of the applied light. The excited electrons in the conduction band may absorb light through free-electron absorption, and they may promote further electrons to the conduction band through impact ionization. Furthermore, the electrons may not have time to relax into less excited states, and very high densities of highly excited electrons may be obtained. If dense enough, this electron cloud may start to behave as a plasma, significantly altering the physical properties of the material. Furthermore, thermal diffusion is strongly limited when applying ultrashort laser pulses. Clearly, very different models are required when treating laser-material interaction with long or with ultrashort laser pulses.

3.3 SIMULATIONS ON LASER-MATERIAL INTERACTION

Simulation of laser-material interaction is a rather complex task. The process is three-dimensional, and if considering material transport, such as convection in a molten material or even ablation, i.e. material removal, the simulations get extremely large and time-consuming. For ultra short laser pulses, many optical, electrical and thermal properties of the materials to be simulated are uncertain and must be applied far from equilibrium, in a material that is under influence of tremendous stress. It was chosen to apply somewhat simplified models in this thesis, in order to gain physical insight while keeping model complexity to a minimum.

For the simulations, one important parameter is the ablation threshold fluence, as this is the fluence required for the process to take place. Criteria for ablation are required in order to determine this ablation threshold. For long laser pulses, it is assumed that material is removed only if some material reaches vaporization temperature. Vaporization will remove material in itself, but it will also create recoil pressure that will expel more material. At fluencies close to the ablation threshold, the majority of the material will be removed through expulsion. This ablation threshold will be valid both for long and ultrashort pulses. With ultrashort laser pulses, there may also exist other ablation mechanisms. These mechanisms are connected to the point where a high number density of excited electrons creates a strongly absorbing plasma in the material. As such, in the case of ultrashort pulses, the second criterion for ablation is when the critical electron density is reached.

Two significant physical mechanisms are left out of the simulations, namely material removal and convection. When material is expelled from the melt pool or in other ways removed from the substrate, it will carry with it some of the laser energy. Furthermore, convection and stirring within the melt pool will alter the dynamics of the process. While it would be interesting to investigate these mechanisms as well, it would be outside the scope of this thesis. Still, some considerations can be made. Convection and stirring only has time to take place for long pulses. Generally, convection and stirring within the melt pool will decrease the vertical temperature gradient within the melt pool. The bottom of the melt pool will be hotter, potentially increasing the melting rate for the solid material surrounding the melt pool. As such, convection and stirring may increase the

obtained depth of the melt pool. At the same time, the surface temperature will be reduced, increasing the threshold for ablation. On the other hand, material removal will carry with it some of the laser energy, reducing the energy stored in the wafer, hence reducing the thermal impact to the wafer. Quantification of these effects would be difficult, however, Mangersnes have performed simulations omitting these effects, still obtaining good correspondence between simulations and experiments. This seems to indicate that the effect of convection and stirring may be minor when seeking to determine the ablation threshold fluence.

For the simulation of both long and ultrashort laser pulses, the partial differential equation solver pdepe was applied. This is included as a standard routine in Matlab. One approximation performed in all simulations is that the physical situation is one- dimensional. This implies that the laser irradiation is homogenous and the laser spot is infinitely large. This is of course not the case, however, the approximation is reasonable. The laser spot is normally on the order of 40 μm in diameter, while the laser energy is deposited within 1 μm from the wafer surface, sometimes within the first 0.1 μm from the surface. As such, the lateral length scale is much larger than the length scale into the substrate.

The pulses were assumed to have a Gaussian temporal distribution, with the pulse duration being the full-width half-maximum (FWHM) duration. The surface reflectivity was set to zero, looking at the optical intensity entering the material. This as the reflectivity can be changed rather arbitrarily by the application of suitable (anti-)reflection coatings.

3.3.1 LONG PULSES

Using long laser pulses, the absorption in the material is given by the linear absorption coefficient of the material. The temperature rise of the material is given by laser energy input, heat capacity and heat conductivity. The heat equation is given by:

$$\frac{\partial U}{\partial T} = C\frac{\partial T}{\partial t} = \frac{\partial}{\partial x}\left(K\frac{\partial T}{\partial x}\right) + \alpha I$$

where U is the thermal energy of the material, C is the heat capacity of the lattice, T is the temperature, K is the thermal conductivity and α and I are the optical attenuation coefficient and intensity respectively. This equation describes how the thermal energy of the system changes as a result of thermal conduction and as a result of energy input from optical absorption. The optical intensity distribution follows the Beer-Lambert law:

$$\frac{dI(t)}{dx} = -\alpha(T)I(x,t) \longrightarrow I(x,t) = I_0(t)\exp - \int_0^x \alpha\big(T(x')\big)\,dx'$$

with a constant α , this expression gives an exponentially decaying intensity. However, α is generally temperature dependent. With temperature dependent α, there is a feedback mechanism. Optical absorption causes a temperature rise, which again causes a change (normally an increase) in absorption by changing α. Phase changes are taken into account by modifying C_S into containing the enthalpy of phase change. The model developed by Mangersnes was applied for simulations on long laser pulses in the visible wavelength range.

3.3.1.1 Long laser pulses at long wavelengths

Semiconductors are generally considered to be transparent, for all practical purposes, for photon energies below the band-gap of the material, as the photon does not carry enough energy to bridge the band-gap. However, in some cases, free-carrier absorption may become relevant. Free carrier absorption is absorption by carriers in the conduction band, and has an absorption coefficient described by

$$\alpha_{fca} = \theta N \qquad 3.3$$

Normally, this effect is very weak, as the number density of conduction band electrons is fairly small. However, if the temperature of the semiconductor is high enough, a significant number of thermally excited electrons will exist. In addition, the free-carrier absorption coefficient 8 generally increases with h^2, meaning that this effect will be very pronounced at long wavelengths. With high temperature substrates and long wavelengths, free-carrier absorption may be strong.

The model developed by Mangersnes was adapted to be suitable for the absorption encountered at a wavelength of 9.3 µm. No experimental investigation was found describing the temperature dependence of the absorption in silicon at 9.3 µm. As such, a theoretical expression was used. The temperature dependence of the free carrier absorption is described as

$$\alpha_{fca}(N,T) = \alpha_{fca}(10^{16},300) \times (N(T))/(10^{16}) \times (\mu(10^{16},300))/(\mu(N,T) \qquad 3.4$$

Here, $\alpha_{fca}(N, T)$ is the free-carrier absorption (FCA), the only contribution to absorption that is taken to be temperature dependent. Starting with FCA at room

temperature, the temperature dependence comes from the temperature dependence of the

number density of conduction band electrons, N(T) and from the temperature dependence of the mobility, μ(N, T). These two quantities have not been investigated close to the melting point of silicon, where the simulations are most sensitive to the value of α_{fca}. This constitutes a serious source of uncertainty in the simulations. Another source of error is the thermal interface resistance between the dielectric and silicon. This quantity is taken to be temperature independent, however, at least when the dielectric melts, the interface thermal resistance must be expected to change. The paper also clearly shows that correspondence between simulations and experiments is rather poor, the only result that should be valid is that shorter pulses will allow for less heat transfer to the silicon substrate.

As for the experimental investigations of laser ablation by CO_2-lasers, the lack of lasers with shorter pulse durations has excluded the exploration of potentially very interesting parameter ranges.

3.3.2 ULTRASHORT PULSES

The term ultrashort pulses has probably arisen from the need of a counterpart to the rather short pulses in the nanosecond range, which are in this context regarded as “long”. Normally, the term “ultrashort pulses” is applied to pulses with a duration in the pico- and femtosecond range. Here, “ultrashort pulses” is taken to mean pulses where non-linear interaction is expected to be a significant part of the physics, but where the assumption that the extension of the pulse is large compared to e.g. optical absorption lengths etc. is still valid. This will hold well for pulse durations down to 0.5 ps, the shortest pulses applied within this thesis, having an extension in silicon of about 35 μm. As described in section 3.2, ultrashort laser pulses call for a different physical model than long pulses. As a result of the potentially different temperature in the electron and lattice systems, two coupled heat equations are required in order to describe the system, one for the electrons and one for the lattice,

$$\frac{\partial U}{\partial t} = \frac{\partial}{\partial x}\left(K\frac{\partial T}{\partial x}\right) - \frac{3Nk}{\tau\,(e-1)}\,(Te - Tl) + q_{tot} \qquad 3.5$$

In equations 3.5 and 3.6, $U_{e/S}$, $T_{e/S}$ and $n_{e/S}$ are the thermal energy, temperature and heat conductivity of the electron/lattice system, respectively. v_{e-S} is the electron-lattice

coupling time, q_{tot} is the total energy input from the laser, N is the number density of conduction band electrons and k_B is the Boltzmann constant. As the number density of electrons is not constant, but is changing through generation and recombination mechanisms, the number density of electrons must be accounted for, adding a third coupled equation:

$$\frac{\partial N}{\partial t} = \frac{\partial}{\partial x}\left(D_0 \frac{\partial N}{\partial x}\right) - \gamma N^3 + \delta N + \sum \frac{a_n I^n}{n\hbar\omega}$$

Here, D_0 is the electron diffusivity, y is the Auger coefficient, ð is the impact ionization coefficient, a_n is the n-th order absorption coefficient and ℏm is the photon energy. The total energy input from the laser is:

$$q_{tot} = \alpha_{eff} I = \left(\sum a_n I^{n-1} + \theta N\right) I \simeq (\alpha + \beta I + \theta N) I$$

where the summation indicates all relevant multi-photon absorption processes, and the last term is the free-carrier absorption. þ is the two-photon absorption coefficient. When working on silicon, linear absorption, two-photon absorption and free-carrier absorption will be the dominant processes. Two-photon absorption is the simultaneous absorption of two photons, and is a mechanism which has an absorption coefficient that is proportional to the optical intensity. Two photon absorption may induce absorption in materials where the photon energy is not high enough to bridge the band-gap, but where two photons combined have sufficient energy, or it may increase absorption significantly in cases where linear absorption is weak, e.g. for photon energies close to the band-gap energy in silicon.

Looking at the equations, it is clear that the laser energy is deposited into the electron system, while the electron-lattice coupling term causes an energy flow between the hotter electron system and the colder lattice system until the two reach equilibrium. Impact ionization and band-to-band absorption cause an increase in the number density of conduction band electrons, while Auger recombination removes electrons. Free-carrier absorption does not contribute to the number density of conduction band electrons, but causes an increase in the temperature of the electron system. The absorption in the medium becomes dependent both on the optical intensity and on the number density of conduction band electrons.

In the model described above, the expressions for optical absorption and assumptions on constant optical reflectivity break down when approaching the critical electron density, as a result of the free-electron contribution to the dielectric constant of the

material. This implies that anything happening to the substrate after this point, such as phase transformations and material removal is not accurately described in the simulations. In fact, the physics behind melting or disordering mechanisms resulting from ultrashort- pulse irradiation of semiconductors is quite complex. Several authors have pointed towards melting of the semiconductor (as opposed to e.g. Coulomb explosion), and that the melting turns non-thermal by ultrafast disordering mechanisms if the laser fluence is sufficiently above the melting threshold. Also breaking of the material resulting from internal stress caused by the strong temperature gradients obtained by ultrashort laser pulses has been suggested as material removal mechanism.

Other mechanisms that are not considered within the two-temperature model are the incomplete thermalisation between optical and acoustic phonons, the electric field arising within the material due to electron emission and modification of material properties due to deformation of the material itself. While these mechanisms have an influence on the interaction dynamics, this thesis focused on obtaining meaningful results while keeping the complexity of the model and the number of uncertain material parameters to a minimum. Results indicate that the main physical mechanisms are included also in the two-temperature model, and that the choice of model as such is a sensible one.

The pdepe solver is able to solve sets of coupled partial differential equations. However, the expression for optical intensity cannot be explicitly obtained, and needs to be found from the integral expression in equation 3.2. In order to make the solution converge, a set of iterations are implemented. Firstly, a temperature distribution and distribution of number density of electrons are set as functions of time and space coordinates, assuming quite limited heating and excitation. From these distributions, the optical intensity is calculated as function of time and space, starting with quite low incoming optical fluence. Then, this optical intensity distribution is used as the source term in the equations. When a solution is found, the temperature and electron distributions are used to re-calculate the intensity distribution, and repeat until the solution converges. Thereafter, the incoming optical fluence is increased by a certain ΔF, and the previously found temperature and electron distributions are again used to calculate the optical intensity distribution, and the procedure is repeated.

These iterations are repeated until one of the criteria for ablation is reached. These criteria are discussed in section 3.3, and are that the lattice reaches vaporization temperature, or that the number density of electrons in the conduction band reaches the

critical electron density, N_{cr}. Then, the ΔF is reduced, until two pulse fluencies are found, one being above the ablation threshold and one below, and the difference between them is lower than 3 %.

3.3.2.1 Some results from the simulations

Figure 3.4 shows the optical intensity normalized to the intensity at the wafer surface as a function of depth into the silicon wafer, in order to illustrate the optical attenuation. The figure shows data for a laser wavelength of 1030 nm, 0.575 J/cm^2 and a substrate temperature of 300 K. The pulse duration is 3 ps (FWHM). Three curves are shown, at 3 ps before the peak of the pulse, at the peak of the pulse, and at 3 ps after the pulse. At 3 ps before the pulse, both the optical intensity and the number density of excited electrons are low, and hence the relatively weak linear absorption dominates. This gives only very moderate absorption. At the peak of the pulse, the optical intensity is very high, and the absorption is dominated by two-photon absorption. At 3 ps after the pulse, the optical intensity is equal to the intensity at 3 ps before the pulse, and linear and two-photon absorption are in principle equal in these two cases. The fact that highest absorption is observed at the trailing end of the pulse indicates that free-carrier absorption is dominant late in the pulse. (Heating of the silicon will increase the linear absorption coefficient late in the pulse, but this effect is less dominant than the effects described above.) It is clear that, at least for the case of IR-irradiation of silicon using ultrashort pulses, the laser energy is confined close to the silicon surface when the laser intensity and number density of electrons rise. Also shown in Figure 3.4 is the same data for a pulse with a laser wavelength of 515 nm. Although the absorption increases with time during the pulse, probably as a result of free-carrier absorption, the difference is less prominent than for 1030 nm laser wavelength.

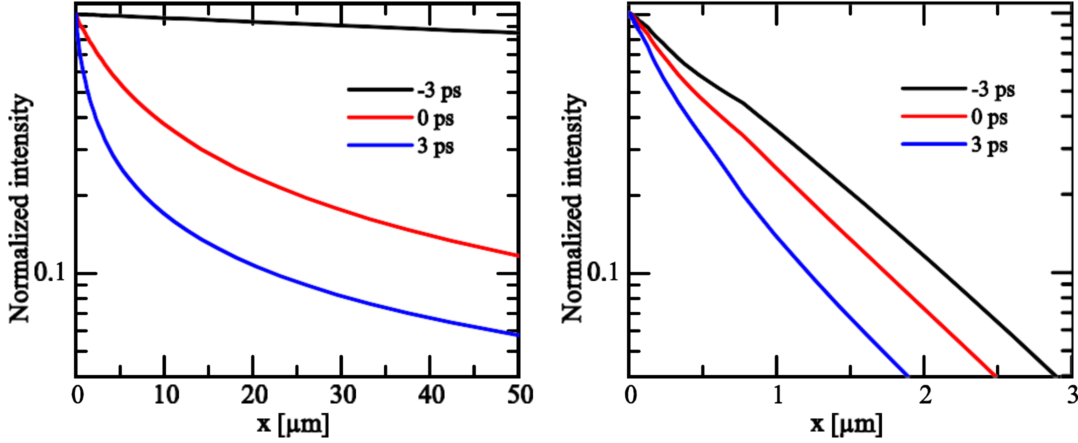

Figure 3.4: Normalized intensity distribution through a silicon slab at various times during a laser pulse of 3 ps duration. The laser wavelength is 1030 nm (left) and 515 nm (right). Non-linear absorption mechanisms are far more prominent for the case of irradiation at 1030 nm, as the linear absorption is quite strong at 515 nm. Note the differences in x-scale.

3.3.3 FREE ELECTRON THEORY

In a dielectric or semiconductor, a high number density of electrons in the conduction band can be generated e.g. by optical excitation. These electrons (and their corresponding holes in the valence band) are quasi-free, and may be described as plasma. The dielectric response of the material will be affected by the presence of such a plasma, and free- electron theory may be applied in order to describe this response. This field shall be reviewed here in some more detail. The dielectric response of a material can, in free-electron theory be described by

$$\epsilon = \epsilon' + i\epsilon'' = \epsilon_{bg}\left(1 - \frac{\tilde{\omega}_p^2}{\omega^2+\gamma^2}\right) + i\,\frac{\epsilon_{bg}\tilde{\omega}_p^2\gamma}{\omega(\omega^2+\gamma^2)} \qquad 3.9$$

where c_{bg} is the background relative permittivity of the silicon material without free carriers. Here, $\tilde{m}_p$ is defined as

$$n + ik = \sqrt{\epsilon},$$

for normally incident light on a substrate with index of refraction n and extinction coefficient k. Depending on the ratio between m, $\tilde{m}_p$ and y, the reflectance as function of number density of electrons can show different shapes. This has effects for laser processing with ultrashort pulses. Figure 3.5 shows the theoretical reflectance curves as functions of electron density in silicon and silicon nitride for the case of irradiation at a wavelength of 515 nm. Silicon has a high index of refraction, giving high reflectivity for the case of low electron densities, while silicon nitride has a lower index of refraction. Now, y is related to the mobility of the material. Using a mobility of 100 cm^2/Vs in silicon (high carrier density), and 1 cm^2/Vs in silicon nitride, it is evident that the reflectance behavior at high electron densities is very different in the two cases.

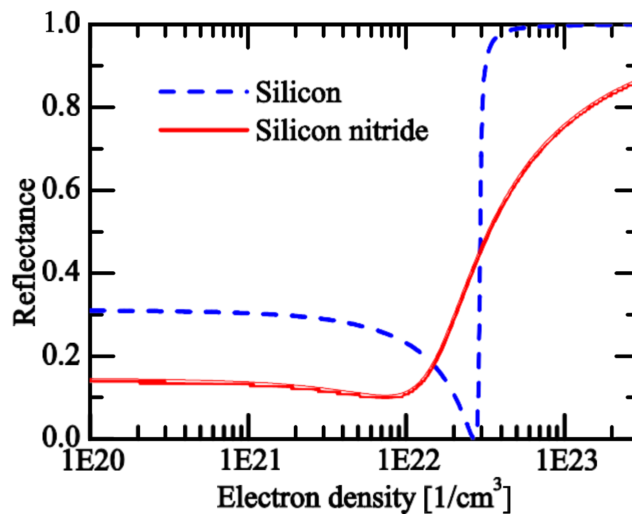

Figure 3.5: Theoretical reflectance as function of free electron density in silicon and silicon nitride. The shape of the curves is very different in the two cases, as a result of the different ratio between m, $\tilde{m}_p$ and y. Silicon has a fairly high electron mobility (resulting in $y \ll m$), while silicon nitride has a fairly low electron mobility (resulting in $y \gg m$). As such, the plasma response in silicon is dominated by the rapidly alternating electrical field, while the response in silicon nitride is dominated by collisions within the material. This difference results in a well-defined plasma frequency in silicon, while the increase in reflectance is much slower for silicon nitride.

The fairly high electron mobility in silicon results in $y \ll m$, while the fairly low electron mobility in silicon nitride results in $y \gg m$. As such, the plasma response in silicon is dominated by the rapidly alternating electrical field, while the response in silicon nitride is dominated by collisions within the material. This difference results in a well-defined plasma frequency in silicon. The reflectance drops when approaching the critical electron density, increasing rapidly to unity thereafter. In this situation, it will be very difficult to introduce more laser energy into the material once the critical electron density has been

reached, as the laser light will be completely reflected. For the case of silicon nitride, on the other hand, the reflectivity varies more slowly. Here, it will always be possible to continue laser energy input.

3.4 LASER INDUCED DAMAGE

When laser processing silicon, the material is normally heated and molten, or in some other way structurally altered. The process result will be a silicon wafer with some degree of crystal damage, as re-crystallization or re-structuring seldom is damage-free. It can be expected that the area influenced by the laser process will be degraded in some way, and this degradation will have a negative influence on the solar cell performance.

In order to get a view on the quality and applicability of the laser process, the laser damage must be quantified in some way.

This section considers methods for characterization of laser induced damage, and the influence on effective minority carrier lifetime from a laser damaged area is analyzed.

3.4.1 CHARACTERIZATION OF LASER-INDUCED DAMAGE IN SILICON

The quality of a solar cell is closely linked to its efficiency, where the highest possible efficiency is desirable. Any process reducing the efficiency of the cell must therefore outweigh this efficiency decrease by some other benefit, often lower production costs. Laser processing of silicon solar cells is one such process with the potential to reduce the efficiency of the cell, and ideally, the efficiency of a cell with laser processing should be compared to a damage-free reference process in order to quantify laser-induced damage. However, it is not always desirable, practical or even beneficial to create complete solar cells and monitor the resulting efficiency, and often more indirect ways of quantifying laser-induced damage are applied. In this section, some methods for characterization of laser damage are discussed.

When looking at a silicon wafer, one important material parameter influencing the potential efficiency of a solar cell made from that wafer is the minority carrier lifetime. Laser damage may reduce this lifetime, decreasing the maximum potential efficiency of the finished solar cell. This reduction in lifetime comes from the introduction of recombination sites, such as various crystallographic defects. Whether using long laser

pulses resulting in melting and recrystallization of silicon or ultrashort pulses where the material processing may take place by ultrafast disordering mechanisms, the resulting crystal quality must always be considered. Especially in the case of ultrashort pulses, one is often lead to believe that the ablation may be completely damage-free, as redistribution of silicon may be suppressed, and the process result may look very smooth and clean. Transmission Electron Microscopy (TEM) is rather frequently used for investigation of laser damage, and may reveal seemingly perfect silicon crystals under such ablation spots. However, TEM is not necessarily the best suited characterization tool for finding defects which may be small and low-concentration. A good example is shown in Figure 3.6. This figure shows TEM images of cross-sections of ablation spots from irradiation by a nanosecond laser at 1064 nm wavelength on an atomic scale. As shown by Engelhart, such a laser produces electrically active defects down to around 25 µm below the wafer surface, while the TEM images show amorphous silicon at the surface of the wafer, and very good crystal quality below a couple of tens of nanometers. TEM is unable to reveal the damage leading to reduced lifetime, which may not be very surprising. As shown, electrically active defects may affect silicon solar cell performance even at defect levels between 10^{11} and 10^{16} 1/cm^3, corresponding to a defect level of less than one ppm (and potentially much lower). Although the density of defects in a laser treated area is unknown, it is not impossible that one is looking for one defect among a million silicon atoms, a task that is impossible for TEM analysis. As such, it seems obvious that electrical characterization is imperative in order to quantify laser damage.

One way of quantifying laser damage is to measure the effective lifetime of a laser-irradiated wafer as described in section 2.7. The laser damage will result in a lowering of the lifetime, potentially revealing information about the extent of the laser damage.

During this thesis, several experiments have been performed ablating SiN_x from silicon wafers using lasers with pulse duration from ~100 ns to 500 fs and from UV to IR, and the effective lifetime of these samples has been measured. However, it was observed in all of these experiments that the effective lifetime was the same, and corresponded to the lifetime of a single sided diffusion limited surface recombination. This behavior shall be discussed in further detail.

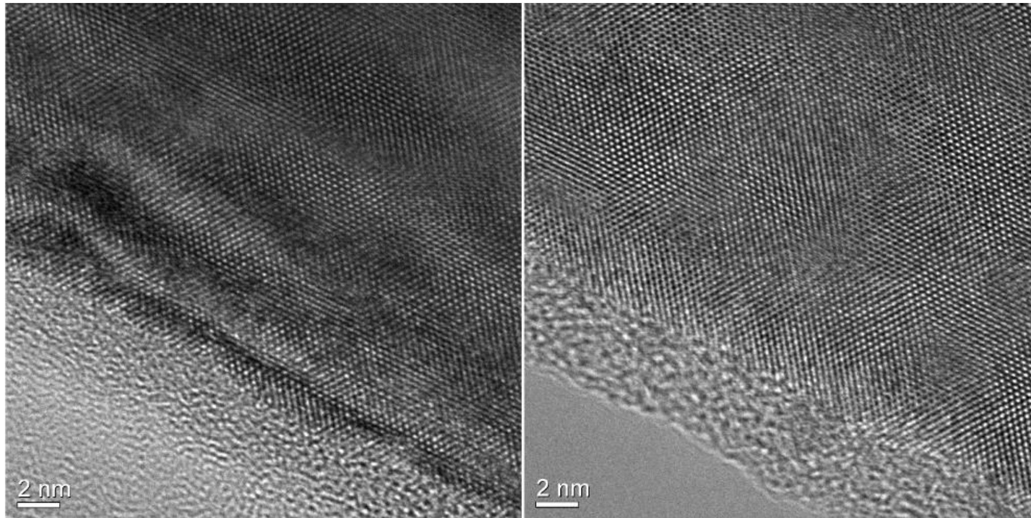

Figure 3.6: TEM images of silicon wafer irradiated by nanosecond pulses with a wavelength of 1064 nm. The images show cross-sections of the laser spot, where an amorphous silicon layer can be observed in the lower-left corners (near the wafer surface), and an ordered silicon crystal in the upper-right part of the images. (TEM performed by Annett Thøgersen, UiO.)

4 LIGHT-TRAPPING STRUCTURES IN SILICON SOLAR CELLS

This chapter motivates the use of light-trapping structures in silicon solar cells and presents the benefits of light trapping. Then, some typical light-trapping structures are shown, followed by a description of some of the alternative routes to fabrication of light-trapping structures using lasers. Thereafter, the approach taken in this thesis to the fabrication of light-trapping structures using lasers is presented. Finally, the results and the applicability of the textures are discussed.

4.1 LIGHT MANAGEMENT IN SILICON SOLAR CELLS

In a solar cell, one major task is to make sure that as much as possible of the incoming sunlight is converted into electricity. In order to achieve this, optical losses must be reduced as much as possible. The effort of reducing these losses is termed light management. Figure 4.1 shows a sketch of possible optical losses in a silicon solar cell. R_f denotes the front surface reflection, which consists of the light being reflected off the front surface without entering the solar cell. R_{ecc} denotes the escape light, light which has entered the solar cell, but is able to escape before being absorbed. Three parasitic absorption mechanisms, absorption that does not generate current in the solar cell, are also indicated. $A_{RefSector}$ denotes optical absorption in an imperfect rear mirror, free-carrier absorption, $A_{FCÆ}$, is the absorption by conduction band electrons, an optical absorption mechanism which does not generate electron-hole pairs. This mechanism is intrinsic to silicon, and is strongest in highly doped silicon, such as in the emitter. Also the anti- reflection coating may absorb some of the incident light, here denoted as $A_{ÆRC}$.

With a quite high index of refraction, bare silicon reflects on the order of 30 % of the incoming sunlight due to Fresnel reflection. In order to reduce R_f, two tricks are normally applied. Firstly, an anti-reflection coating can be applied to the surface, consisting of a transparent layer with a thickness of h/4 and an index of refraction ideally equal to $\sqrt{n_{Si}}$, thus minimizing or eliminating reflection at the target wavelength, and significantly reducing overall reflection. (For an introduction to Fresnel and thin-film optics.) Typically, when weighting the reflectance spectrum with the AM1.5 spectrum, integrating over a 300 – 1200 nm wavelength range, an integrated reflectance of
around 10 % can be achieved by application of an anti-reflection coating. Secondly, texturing of the surface may further increase the optical coupling into the silicon. If the light experiences multiple bounces off the silicon surface, each bounce will reduce the total reflectance.

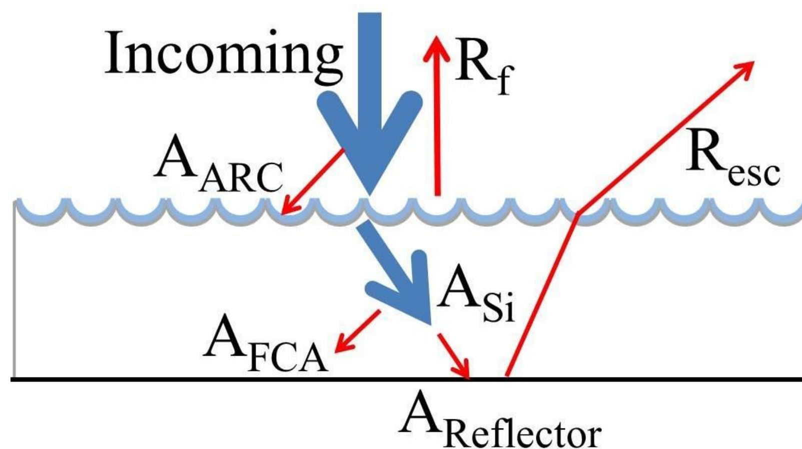

Figure 4.1: Sketch of a wafer showing various contributions to optical absorption and loss in a solar cell. The rear reflector is shown in black, while the anti-reflection coating is shown in blue. A_{Si} denotes the silicon absorption, the only absorption mechanism generating electron-hole pairs. The optical loss is divided into front side reflectance, R_f, escape light, R_{esc}, absorption in the rear reflector, $A_{Reflector}$, absorption in the AR-coating, A_{ARC}, and absorption by free carriers, A_{FCA}

Silicon is an indirect band-gap semiconductor, meaning that the optical absorption process must be assisted by absorption or emission of a phonon for momentum conservation. This characteristic makes silicon a rather poor optical absorber. While other solar cell materials may show acceptable absorption in a 1 μm thick absorber, silicon requires quite long absorption lengths. This trend is especially clear for photon energies near the band-gap energy of silicon.

In Figure 4.2 (left), the attenuation coefficient and optical penetration depth in silicon is shown. The optical penetration depth is defined as the distance the light has to

travel through silicon in order to be attenuated to 1/e intensity level. The hatched range is a range of penetration depths ranging from 160 µm to 20 µm. 160 µm is around the current industry standard wafer thickness, while 20 µm corresponds to a realistic long-term target thickness. It is seen that wavelengths above approx. 800 nm will have the possibility to penetrate the thinnest of these wafers, the penetration depth easily reaches several millimeters at wavelengths above 1100 nm, meaning that the light can travel much further than the thickness of the wafer before being absorbed. It is at wavelengths showing a penetration length on the order of, or longer than the thickness of the wafer that contributions to R_{esc} are expected. In order to reduce loss contributions from R_{esc}, the path length of the light through silicon must be increased. The act of increasing the path length is often called light trapping. Figure 4.2 (right) shows the photogenerated current, J_{ph} generated from band-to-band absorption by sunlight (AM1.5) passing through a given path length in silicon. Optical losses occur even to optical path lengths exceeding 1000 µm.

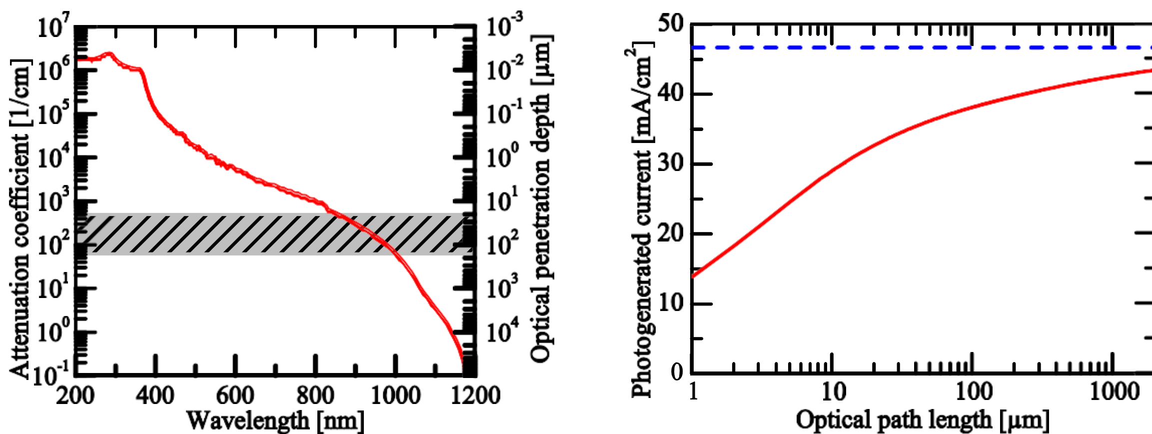

Figure 4.2: Left: The optical attenuation coefficient and corresponding optical penetration depth in silicon as function of wavelength. Also indicated is a relevant range of wafer thicknesses for solar cell applications. The need for light-trapping for wavelengths above 800 – 1000 nm depending on wafer thickness is obvious. Right: The photogenerated current from sunlight (AM1.5) absorbed by a given path length in silicon (solid line). Also indicated is the maximum current available (dashed line).

Figure 4.3 shows a collection of light-trapping strategies. A shows a planar silicon slab with no rear reflector, where the light gets only one straight pass through the wafer. This must be considered as an absolute worst case scenario. B shows a planar structure with a rear reflector, ensuring two straight passes through the wafer. In a solar cell, the rear metal contact often acts as a mirror (although not a perfect one). C shows a front side textured structure, where the path length in the silicon is increased as a result of the oblique angle taken by the light passing through the wafer. A high probability of escape after two passes is indicated. In silicon, any light hitting the silicon / air interface will be totally

internally reflected if the incidence angle 8_i is larger than $8_i = \sin^{-1}(n_1/n_2)$, which for silicon in air, at wavelengths near the band-gap equals approx. 16.5°, a fairly shallow angle. Angles below 16.5° are referred to as the escape cone, as light within this cone will have a high probability of escaping the silicon wafer.

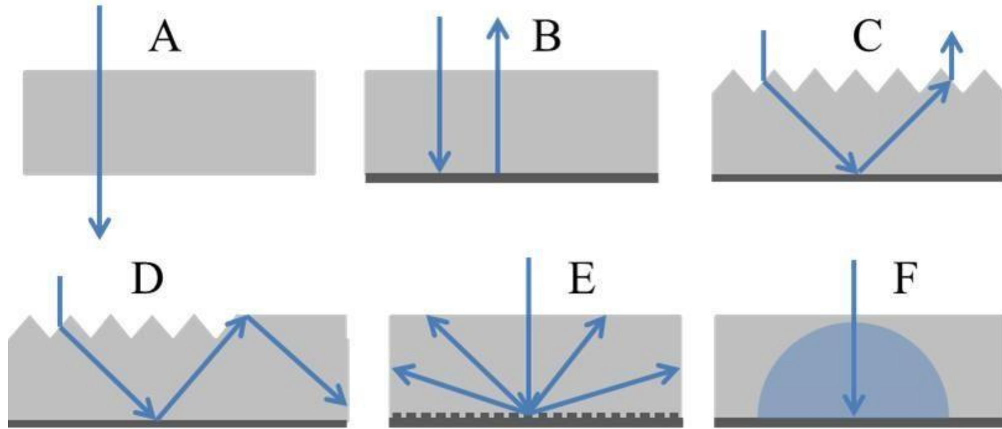

Figure 4.3: Sketch of various light-trapping schemes. A - no light trapping, B - rear reflector, C – front surface texture, D – symmetry-breaking front side texture, E – diffractive rear reflector, F – Lambertian rear reflector.

D and E are examples of more advanced light-trapping structures. In D, a textured surface is shown, but unlike C, the symmetry of the texture is broken. Created correctly, such symmetry-breaking structures can cause most of the light to hit the wafer surfaces at angles outside the escape cone, thereby causing total internal reflection to be dominant, and multiple passes are ensured for the majority of the light. E is meant to indicate a diffractive rear reflector, where the incoming light is diffracted into several diffraction orders. The angle of the diffraction orders can be tuned by varying the grating period so that total internal reflection is ensured for all but the specular diffraction order. If, in addition, the specular order is suppressed, the light trapping can be very efficient. F is meant to indicate the case of Lambertian light trapping. Lambertian light trapping is an idealized theoretical light-trapping scheme, where a perfect rear reflector reflects the light homogenously in all directions, independent of the angle of the incoming light. It can be shown that the Lambertian light trapping is the maximum achievable light trapping for a sample uniformly illuminated from all directions. The path length of light in a Lambertian light-trapping scheme can be calculated to $4wn^2$, where n is the refractive index of the material and w is the wafer thickness. In silicon, this path length enhancement $4n^2$ is about a factor 50. While light-trapping is not critical in thick wafers, Figure 4.2,(right) shows that thinner wafers benefit strongly from light-trapping. Increasing the path length

in a wafer from 20 μm by the Lambertian factor to 1000 μm would increase the photogenerated current from around 70 % of the available photocurrent to above 90 %.

The industry standard for mono-crystalline silicon texturing is today the double- sided random pyramid structure. This is created by etching a <100>-oriented silicon wafer in a diluted KOH solution, often adding an alcohol for improved quality of the texture. Such an etch preferentially exposes the <111> crystal planes, leaving a random pattern of upright pyramids. This texture shows a low front surface reflectance, due to the steep angles of the pyramids, and also shows very decent light trapping, as there will be a strong randomization of the direction of the light when refracted or reflected off the various pyramid facets. For multi-crystalline silicon, the random pyramid texture is less efficient, as the direction of the pyramids is dependent of the crystal orientation of the wafer. Therefore, for multi-crystalline wafers or mono-crystalline wafers with e.g. a <111> orientation, isotropic acidic etching is normally applied. This texture will form random dimple-like structures. As the dimples are generally flatter than the pyramids, the chance of experiencing multiple bounces off the front surface is limited, and the front surface reflectance is significantly higher than for the random pyramids. The light-trapping properties, however, are rather good.

Common for both of these textures, is that they require some form of seeding or attack points in order to form uniformly. Such seed points are readily available today, as most wafers are cut by wire sawing, where the saw damage generates seed points. However, several new wafering technologies are emerging, where no saw damage is present. This poses a challenge for the traditional texturing methods. Furthermore, wafer thickness is expected to decrease, caused by a need to reduce silicon consumption and silicon costs. The traditional texturing methods will remove significant wafer thickness, being less suitable for thin wafers. To overcome these hurdles, new texturing methods must be developed. This thesis presents two ways of creating light management structures on silicon by laser assisted methods.

4.2 STATE OF LASER TEXTURING

Already, several approaches to laser texturing of silicon exist. These will be briefly reviewed in this section, and a motivation is given for the approach to laser texturing taken in this thesis.

Black silicon

So-called black silicon can be created by irradiation of a silicon surface using ultrashort laser pulses. If a single spot is irradiated by multiple pulses, self-assembling structures tend to emerge, shown in Figure 4.4 (left). Such structures are often created in a sulfur hexafluoride (SF_6) – atmosphere, but they may also be created in air. Black silicon, as the name suggests, displays an extremely low reflectivity over the whole relevant wavelength range, and is as such very close to the ideal anti-reflection coating. On the more practical side, one obstacle seems difficult to bridge. In articles describing black silicon formation, typical parameters may be: Pulse energy density 0.9 J/cm^2, repetitions 300. Using these numbers and multiplying by the size of a 5 inch wafer, a total laser energy of around 44 kJ is required. In current production, 1 wafer/second (or more) is the benchmark for a relevant process. In order to deliver 44 kJ of energy to a wafer in such a short period of time, one would need a 44 kW laser. Not only are such lasers far away from state of the art, but even if one could find such a laser, it would be very interesting to see how a silicon wafer would react to such a violent energy input. With very little material removal, the majority of the laser energy must remain in the silicon wafer. Using the heat capacity and melting enthalpy of silicon, 44 kJ is the energy required to heat and melt a 5 inch wafer with a thickness of around 350 µm. Another issue when working with black silicon in general is the very large surface area that is created. The passivation of such a surface must be of very high quality in order for surface recombination not to be a serious problem. Passivation of black silicon surfaces by the use of atomic-layer deposited Al_2O_3 is showing promising results.

Laser Drilling

A second option for laser texturing is simply to drill a suitable geometric structure, such as the honeycomb structure in mc-silicon shown in Figure 4.4 (middle). Holes are drilled, and thereafter, the structure is etched in order to remove the laser damaged areas and debris from the process. While this process significantly reduces front surface reflectance for mc-silicon, material removal by laser ablation is an energy intensive process. In this case, 10 J/cm^2 and 3 repetitions were applied. Assuming an effective area coverage of 25 % (the 10 J/cm^2 would not be applied to the whole surface), the required energy for texturing of a 5 inch wafer is around 1 kJ. While this is much better than what was the case for black silicon, and in a range where industrial lasers do exist, this is still quite a lot of energy to put into a wafer within one second.

Masked laser processing

A third option for laser processing is masked laser processing, shown in Figure 4.4 (right). Here, a SiN_x etch barrier has been applied to the wafer, and the laser is applied only for creating openings through the barrier. A wet-chemical etch (in this case an isotropic etch) is applied for material removal and structure development. By this approach, the laser does virtually no material removal, and much lower laser energy can be applied. Typical pulse energies required for silicon nitride removal is around 0.7 J/cm^2. With an area coverage of around 10 % (the image shown has an area coverage of around 5 %), the energy required for opening the etch barrier on a 5 inch wafer is around 10 J, corresponding to a 10 W laser for 1 wafer / second. This is indeed feasible laser power, and easily available today. This masked approach also uses a diffractive optical element (DOE) in order to create several openings through the etch barrier per laser pulse. This relaxes the demand for accurate, high speed scanning and high repetition rate lasers. The requirements on pulse energy rise with the number of spots per pulse, but lasers tend to have pulse energies easily allowing for a high number of simultaneously processed holes.

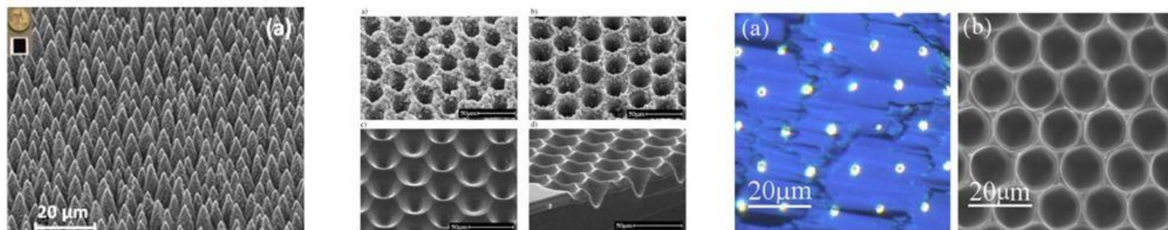

Figure 4.4: Images of black silicon structure (left), laser drilled texture (middle) and masked texture with etching (right).

4.3 MASKED LASER TEXTURING

Masked laser texturing followed by wet chemical etching seems to be the most promising approach to laser texturing of silicon. Firstly, as the estimations above show, it is the process requiring the absolutely lowest laser power for relevant process speeds. Of course, also the time needed for etching must be taken into account, however, wet chemical etching can be performed as a batch process, significantly reducing processing time per wafer. Secondly, if done properly, the etch process may remove any laser damage, ensuring that the texturing process is free of laser damage. Thirdly, wet-chemical etching is extensively used in solar cell processing, and is as such a well-known process. Therefore, masked texturing followed by wet-chemical etching is the approach chosen in this thesis. Two structures have been created, with strongly differing characteristics. The structures are

referred to as the patch texture and the diffractive structure. SEM micrographs of these textures are shown in Figure 4.5.

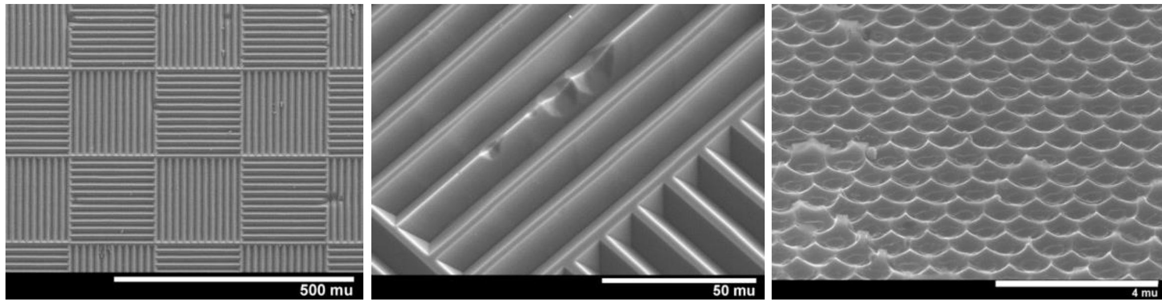

Figure 4.5: Patch texture (left, center). Diffractive dimple structure (right).

In order to predict the performance of geometric light-trapping structures, the ray-tracing program was used, where the performance of the patch texture was investigated.

Diffractive structures receive their properties from interference effects, and ray-tracing is no longer an adequate method.

4.3.1 PATCH TEXTURE

In a series of articles, Campbell investigated several light-trapping schemes for monocrystalline silicon. One of these schemes has the potential to outperform the random pyramid texture, and at the same time be quite insensitive to the angle of the incoming sunlight, namely the patch texture. This texture would be an interesting alternative to today's industry standards.

The patch texture is schematically shown in Figure 4.6 (left). It consists of patches of trenches oriented alternatingly along orthogonal directions. The size of the patch is adjusted to the thickness of the wafer in such a way that the light which is reflected off the rear reflector hits the neighboring patch (as indicated by the white arrow), where the direction of the trench ensures total internal reflection. In this way, the light is trapped very efficiently. As the angle traveled by the light inside of the silicon wafer is only weakly dependent on the angle of the incident light, the light-trapping properties will be largely preserved also at other angles of incidence. The drawback with the patch texture is of course that it requires some kind of masked etching in order to develop the desired pattern.

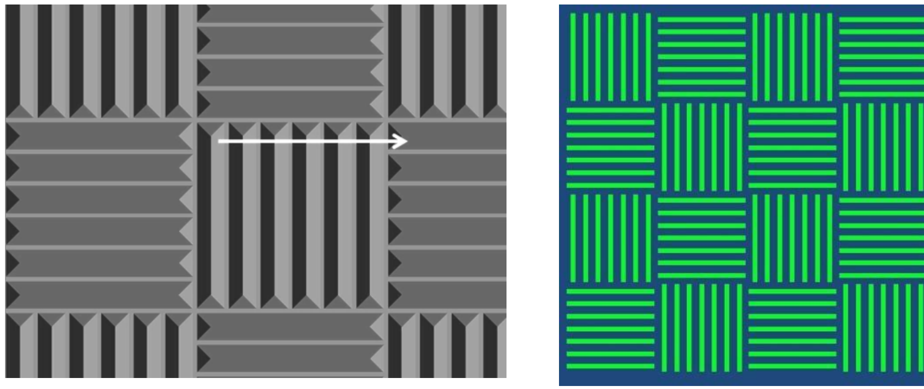

Figure 4.6: Sketch of the patch texture (left). Indicated by the white arrow is the function of the texture, namely that light hitting a point on one patch will hit the front surface at the corresponding point in the neighboring patch, whereby total internal reflection is ensured. Also shown is the pattern which must be opened through the etch barrier for development of the texture (right).

The patch texture is scalable, making it possible to start with relatively large structures as a proof-of-concept, developing the process gradually, reducing feature sizes. SiN_x was chosen as the etch barrier, as SiN_x shows high stability in KOH solutions. Patch textures were created opening the etch barrier locally by laser irradiation. An anisotropic KOH etch then developed the pattern.

It was found that the patch texture, under some circumstances, can deliver higher Jcc than the random pyramid texture taken as reference. The improvement, however, is fairly modest as a result of the fact that the random pyramid texture is a very good light- trapping structure. It has a low front surface reflectance and decent path-length enhancement. This, combined with the simplicity of the random pyramid texturing process makes it a hard reference to beat. Furthermore, the performance of the patch texture improves when reducing the feature sizes. This, in turn, puts great demands on the performance of the laser system. Single laser pulses were applied, and the pattern was drawn using a xy-table for translation. This is a very slow process, not at all industrially suitable. A galvo scanner would increase scanni ng speed, but only to a certain degree. A patch pattern with 5 µm wide trenches would require a line somewhat longer than 3 km to be written on a 5 inch wafer, a formidable task even if disregarding accuracy and the fact that it is not simply a straight, continuous line that has to be written. The use of a diffractive optical element (DOE) or other beam-shaping element would have to be applied for industrially relevant implementation of the process. Figure 4.6 (right) shows an image of the laser pattern required for the creation of a patch pattern. If an area on the wafer of 400x400 µm could be processed with one pulse, a laser with 100 kHz repetition rate and a

scan speed of 40 m/s would be required. These are still rather strict requirements for a laser system, but more feasible than the one spot per pulse alternative.

The second challenge related to the small feature sizes is the positioning accuracy and accuracy of the laser intensity and demands on positioning accuracy rises with decreasing feature size. A further benefit of using a DOE is that the requirement for relative positioning accuracy between spots would also be greatly reduced, as one spot would cover a larger area. Furthermore, small features require tight laser foci. Tight foci have small focal depth, meaning that the distance to the wafer must be very well controlled in order for the laser fluence to remain within process tolerances. The process would be simplified if using an etch barrier that can be deposited without the need for vacuum processing, such as e.g. spin-coating.

5 DISCUSSION AND OUTLOOK

In this chapter, a discussion of the work in this thesis is given, along with suggestions on the possible continuation of this thesis.

On the topic of light trapping, the high quality of laser-based texturing processes has been demonstrated. The main weakness of this work does not lie in the performance of the textures, but in the complexity of the production processes. In order to achieve the required process speeds, the patch texture requires the use of a diffractive optical element in order to process larger areas with each laser pulse, as discussed.

For the diffractive honeycomb structure, large laser spots can be utilized, and much lower positioning accuracy is required. As such, the laser processing stage is not the critical part of this process. Here the deposition and use of microspheres for the focusing of the laser light is the major obstacle for industrial application. If the microspheres were to be replaced by a re-usable microlens array, the process would be simplified significantly. Both texturing processes would benefit from the implementation of an etch barrier deposition technique that is simpler than the PECVD deposition used within this work. The implementation of the two textures in solar cells would constitute final evidence that the textures have a positive overall influence on a complete solar cell.

On the topic of laser-material interaction, a series of investigations have been undertaken within this thesis, and several interesting and directly applicable findings have been made. The continuation of this work could follow several paths, either towards further fundamental studies and simulations, or towards more application oriented studies. As a direct continuation of the work presented, short pulse, long wavelength laser ablation should be investigated further. E.g. optical parametric oscillators (OPOs) could be able to produce pulses significantly shorter than the 100 ns tested herein, with a tunable laser wavelength. Such lasers would be a powerful tool for investigation of long wavelength laser ablation, provided that they deliver sufficient pulse energy. Alternatively, or in parallel, improvement of the simulation models would lead to better prediction of the parameter ranges required for ablation of dielectrics without silicon substrate melting. As

simulation results are no more accurate than the physical parameters used in the simulations, it would be beneficial to acquire more detailed knowledge on the temperature dependence of several critical parameters used in the simulations. E.g. thermal properties of the dielectrics and free-carrier absorption coefficients have not been explored at temperatures close to the melting temperature of silicon.

As a continuation of the work on ablation of silicon nitrides, the practical differences between direct and indirect ablation of silicon nitrides should also be investigated further. Both the minority carrier lifetime of the substrate and the specific contact resistance of metallizations applied through the contact openings should be investigated for both direct and indirect ablation

It has been demonstrated within this thesis that several important laser processes yield some degree of laser damage. However, the location of the laser damage also affects to which degree the solar cell performance is affected. As such, it would be interesting to perform a thorough analysis of the influence of the geometry of the laser damage on solar cell performance. A comparison of laser damage in the bulk, emitter, and space charge region and directly under contacted areas would be interesting in order to extract the acceptable level of laser damage in each of the cases.

Instead of trying to develop low laser damage processes, it could also be possible to repair laser damage after it has occurred. Thermal annealing and hydrogen plasma annealing of laser induced damage has been characterized by the use of deep- level transient spectroscopy (DLTS), showing the successful removal of laser damage to below the detection limit of the DLTS measurements.

For solar cell applications, the minority carrier lifetime is the relevant measurement quantity, and an investigation of the minority carrier lifetime after such annealing would be interesting. If post-treatment such as annealing is capable of restoring also the minority carrier lifetime in silicon wafers, this could be a very promising tool for enabling low damage laser process

6 CONCLUSION

This thesis had two main objectives. The first objective was to gain fundamental understanding of the interaction between pulsed lasers and materials relevant for silicon solar cells, with an emphasis on parameter ranges leading to ablation. The understanding of laser-material interaction is important from a fundamental point of view, as it forms the basis for the successful development of laser processes. The second objective was to develop laser-based techniques for manufacturing of efficient light-trapping textures. Emphasis was to be on the investigation of the practically achievable quality of textures already explored theoretically in literature. Light-trapping structures are highly relevant for silicon solar cells, considering the decrease industry standard of wafer thickness and the new emerging wafering technologies.

On the topic of light trapping, two processes were developed for the production of two light-trapping structures, namely the patch texture and the diffractive honeycomb texture. The performance of these textures was investigated by optical absorption and transmission measurements, and compared with reference textures. It was found through simulations that the patch texture gives an increase in J_{cc} of up to 0.5 mA/cm^2 compared to the random pyramids texture. The diffractive honeycomb structure delivered a photogenerated current of 38 mA/cm^2 on 21 µm thick silicon wafers. The lack of industry standard methods makes comparison somewhat arbitrary, but at a wafer thickness of 100 µm, the diffractive honeycomb structure gives an increase in J_{ph} of 2 and 4 mA/cm^2 when compared to isotropically etched and polished samples, respectively. As such, it was clearly shown that laser based texturing may provide highly efficient light-trapping structures suitable for thin substrates, including substrates with a crystal orientation different than the <100> orientation.

On the topic of laser-material interaction, several investigations have been undertaken. The investigations, while focusing on different topics, all revolve around the topic of ablation mechanisms. The four papers on laser-material interaction focus on:

Temperature dependent ablation of silicon, ablation of silicon nitrides, laser damage resulting from ablation and ablation of dielectrics using long wavelength lasers.

In order to understand the interaction between ultrashort pulse lasers and the silicon substrate, a simulation model known as the two-temperature model was implemented. In experiments, it was found that the ablation threshold of silicon is dependent on the temperature of the silicon substrate. At a laser wavelength of 1030 nm, the ablation threshold is reduced from 0.43 J/cm^2 at room temperature to 0.24 J/cm^2 when the substrate temperature is 320 °C. The simulation model reproduced the experimental trends. Combining results from experiments and simulations, it was found that a high number density of electrons in the silicon substrate causes the ablation, rather than substrate melting and vaporization as would be the case for pulses in the nanosecond range. For practical applications, the use of a slightly elevated substrate temperature can significantly reduce the required laser power, or correspondingly increase the process throughput. The largest reduction in ablation threshold is observed with a laser wavelength of 1030 nm making this wavelength comparably more interesting. As the use of this wavelength eliminates the need for wavelength conversion stages, the complexity of the laser equipment may be reduced.

The differences in interaction between silicon and long (ns) and ultrashort (ps) laser pulses were investigated through the characterization of the depth of the laser induced damage. It was found that the depth of the laser-induced damage is considerably smaller when applying ultrashort laser pulses than when applying long pulses, being reduced from around 3 μm when using long pulses to around 0.25 μm when using ultrashort pulses at a laser wavelength of 532 nm. This is a result of stronger thermal and optical confinement of the laser energy. An estimate on the minority carrier lifetime in the laser irradiated areas is also presented. Knowledge about the depth of laser damage as function of pulse duration and wavelength is a valuable tool when seeking the right laser for a given process.

When investigating the interaction between various silicon nitrides and ultrashort laser pulses, it was found that, using a laser wavelength of 532 nm, the laser energy was deposited either in the silicon or in the dielectric, depending on the laser pulse duration and the composition of the silicon nitride. Low refractive index nitrides or long laser pulses gave indirect ablation, while high refractive index nitrides or short pulses gave direct ablation. The possible absorption mechanisms were investigated, pointing towards significant interaction between the laser pulse and a dense electron-hole plasma in the silicon nitride. As direct and indirect ablation give differing process results, detailed

knowledge on the ablation behavior of silicon nitrides with varying composition as function of laser pulse duration and laser wavelength is valuable for process development.

The use of long wavelength lasers for the ablation of dielectrics from silicon was investigated theoretically and experimentally, as long wavelength lasers may be absorbed directly in the dielectric, without being absorbed in the silicon. Simulations predict that short laser pulses would provide ablation with minimal heating of the silicon. Experiments using a CO_2-laser operating at a wavelength of 9.3 µm with a pulse duration of 100 ns, however, shows silicon melting, and hence too strong silicon heating. As such, the concept remains to be proven.

This thesis brings contributions to the understanding of the interaction between laser pulses, in particular ultrashort laser pulses, and silicon and dielectrics. This fundamental knowledge adds to the previous literature on the topic, and may serve as basis both for further fundamental studies and for process development. On the topic of light- trapping, two laser based methods are developed for the production of geometric and diffractive light-trapping structures on silicon. It is shown that high-quality light-trapping textures may be produced by laser based processes.

REFERRENCES

[1] P. Engelhart, S. Hermann, T. Neubert, H. Plagwitz, R. Grischke, R. Meyer, et al., Laser Ablation of SiO2 for Locally Contacted Si Solar Cells With Ultra-short Pulses, Progress in Photovoltaics: Research and Applications. 15 (2007) 521–527.

[2] Jostein Thorstensen, Department of Physics Faculty of Mathematics and Natural Sciences, University of Oslo, March, 2013

[3] K. Mangersnes, Back-contact back-junction silicon solar cells, University of Oslo, 2010.

[4] A. Knorz, M. Peters, A. Grohe, C. Harmel, R. Preu, Selective Laser Ablation of SiNx Layers on Textured Surfaces for Low Temperature Front Side Metallizations, Progress in Photovoltaics: Research and Applications. 17 (2009) 127–136.

[5] M. Ametowobla, Characterization of a Laser Doping Process for Crystalline Silicon Solar Cells, Universität Stuttgart, 2010.

[6] D. Bäuerle, Laser Processing and Chemistry, 3rd ed., Springer, Berlin Heidelberg, 2000.

[7] S. Huang, X. Ruan, X. Fu, H. Yang, Measurement of the thermal transport properties of dielectric thin films using the micro-Raman method, Journal of Zhejiang University SCIENCE A. 10 (2009) 7–16.

[8] B. Kuo, J. Li, A. Schmid, Thermal conductivity and interface thermal resistance of Si film on Si substrate determined by photothermal displacement interferometry, Applied Physics A. 55 (1992) 289–296.

[9] W.M. Haynes, ed., Physical Constants of Inorganic Compounds, in: CRC Handbook of Chemistry and Physics, 92nd ed. CRC Press/Taylor and Francis, Boca Raton, FL, 2012.

[10] Y. Cerenius, Melting-Temperature Measurements on, Journal of the American Ceramic Society. 82 (1999) 380–386.

[11] C.L. Yaws, Yaws' Handbook of Thermodynamic Properties for Hydrocarbons and Chemicals, Knovel, 2009.

[12] A. Jain, K.E. Goodson, Measurement of the Thermal Conductivity and Heat Capacity of Freestanding Shape Memory. Thin Films Using the 3ω Method, Journal of Heat Transfer. 130 (2008) 102402.

[13] C.K. Ong, H.S. Tan, E.H. Sin, Calculations of Melting Threshold energies of crystalline and amorphous materials due to pulsed-laser irradiation, Materials Science and Engineering. 76 (1986) 79 – 85.

[14] H. Kobatake, H. Fukuyama, I. Minato, T. Tsukada, S. Awaji, Noncontact measurement of

thermal conductivity of liquid silicon in a static magnetic field, Applied Physics Letters. 90 (2007) 094102.

[15] D.K. Schroder, R.N. Thomas, J.C. Swartz, Free Carrier Absorption in Silicon, IEEE Transactions on Electron Devices. 25 (1978) 254–261.

[16] J. Nelson, the Physics of Solar Cells, Imperial College Press, UK, 2003.

[17] E.H. Sin, C.K. Ong, H.S. Tan, Temperature Dependence of Interband Optical Absorption of Silicon at 1152, 1064, 750 and 694 nm, Physica Status Solidi (a). 199 (1984) 199–204.

[18] N.D. Arora, J.R. Hauser, D.J. Roulston, Electron and Hole Mobilities in Silicon as a Function of Concentration and Temperature, IEEE Transactions on Electron Devices. ED-29 (1982) 292–295.

[19] P. Campbell, S. R. Wenham, and M. A. Green, “Light trapping and reflection control with tilted pyramids and grooves,” in Conference Proceedings of the 20th IEEE Photovoltaic Specialists Conference, 1988, pp. 713–716.

[20] P. Campbell and M. A. Green, “High performance light trapping textures for monocrystalline silicon solar cells,” Solar Energy Materials and Solar Cells, vol. 65, no.1–4, pp. 369–375, Jan. 2001.

[21] E. Hecht, Optics, 4th ed. San Francisco, CA: Addison Wesley, 2002. BIBLIOGRAPHYJ. Gjessing, E. S. Marstein, and A. Sudbø, “2D back-side diffraction grating for improved light trapping in thin silicon solar cells,” Optics express, vol. 18, no. 6, pp. 5481–5495, Mar. 2010.

[22] J. Gjessing, A. S. Sudbø, and E. S. Marstein, “Comparison of periodic light-trapping structures in thin crystalline silicon solar cells,” Journal of Applied Physics, vol. 110, no.3, p. 033104, Aug. 2011.

[23] J. Gjessing, A. S. Sudbø, and E. S. Marstein, “A novel back-side light-trapping structure for thin silicon solar cells,” Journal of the European Optical Society: Rapid Publications, vol. 6, p. 11020, 2011.

[24] S. H. Zaidi, J. M. Gee, and D. S. Ruby, “Diffraction grating structures in solar cells,” in Proceedings of the 28th IEEE Photovoltaic Specialists Conference, 2000, pp. 395–398.

[25] H. Hauser, A. Mellor, A. Guttowski, C. Wellens, J. Benick, C. Müller, M. Hermle, and B. Bläsi, “Diffractive Backside Structures via Nanoimprint Lithography,” Energy Procedia, vol. 27, no. 2011, pp. 337–342, 2012.

[26] B. Bläsi, H. Hauser, O. Höhn, V. Kübler, M. Peters, and A. Wolf, “Photon Management Structures Originated by Interference Lithography,” Energy Procedia, vol. 8, pp. 712–718, Jan. 2011.

[27] E. Haugan, H. Granlund, J. Gjessing, and E. S. Marstein, “Colloidal crystals as templates for light harvesting structures in solar cells,” Energy Procedia, vol. 10, pp. 292–296, 2011.

[28] K. Piglmayer, R. Denk, and D. Bäuerle, “Laser-induced surface patterning by means of microspheres,” Applied Physics Letters, vol. 80, no. 25, pp. 4693–4695, 2002.

[29] A. Barhdadi and J. C. Muller, “Electrically Active Defects in Silicon after various Optical Thermal Processing,” Rev. Energ. Ren., vol. 3, pp. 29–38, 2000.

[30] E. M. Lawson and S. J. Pearton, “Hydrogen passivation of laser-induced acceptor defects in p-type silicon,” Physica Status Solidi (a), vol. 72, pp. 55–58, 1982.

[31] J. L. Benton, C. J. Doherty, S. D. Ferris, D. L. Flamm, L. C. Kimerling, and H. J. Leamy, “Hydrogen passivation of point defects in silicon,” Applied Physics Letters, vol. 36, no. 8, 1. p. 670, 1980.